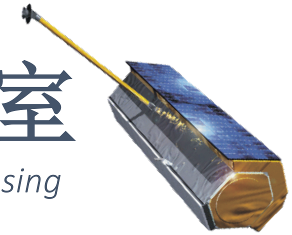

Synthetic Aperture Radar Tomography

Timo Balz, Stefano Tebaldini, Laurent Ferro-Famil

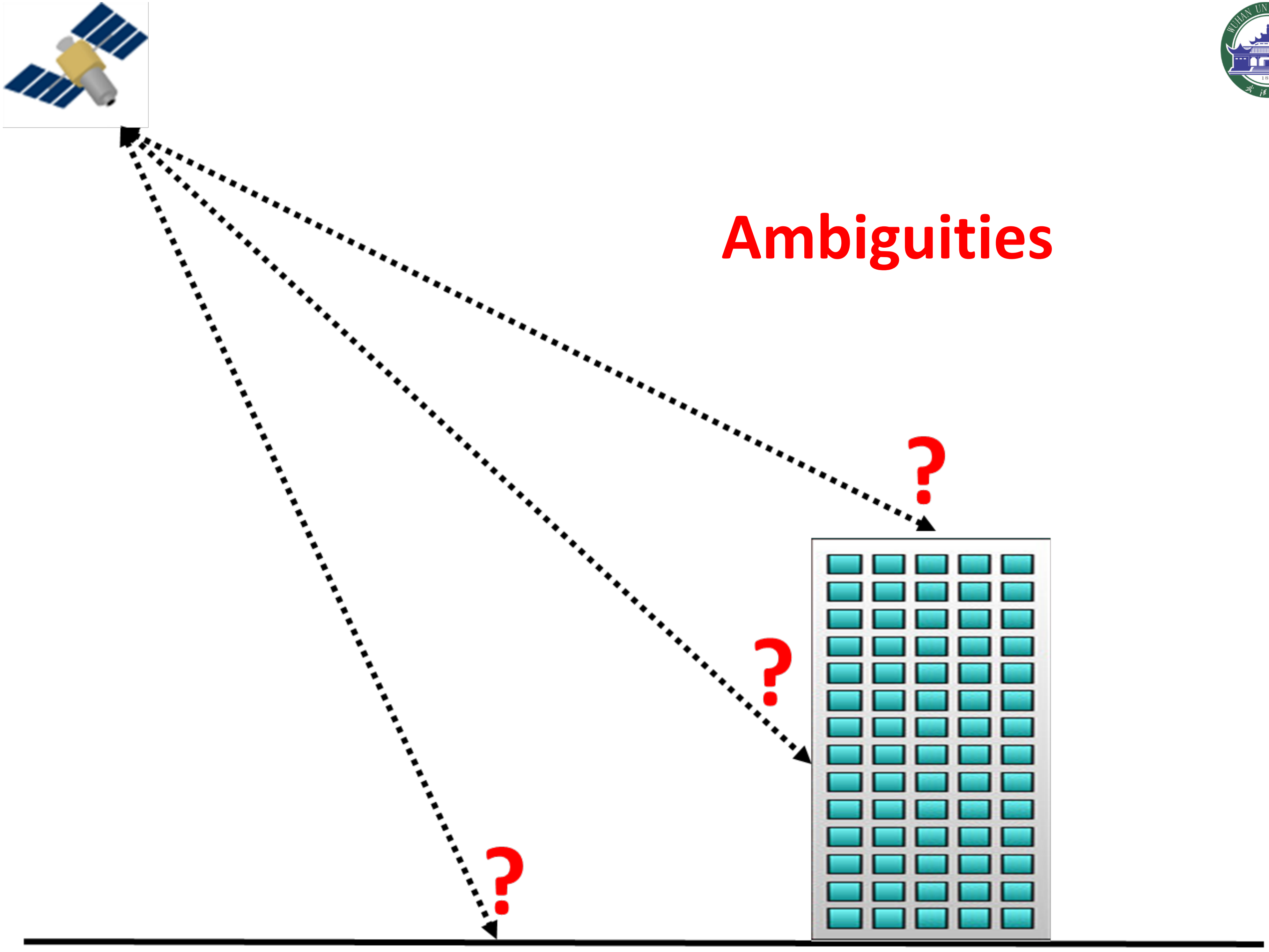
Ambiguities
?
?
?

TomoSAR principle

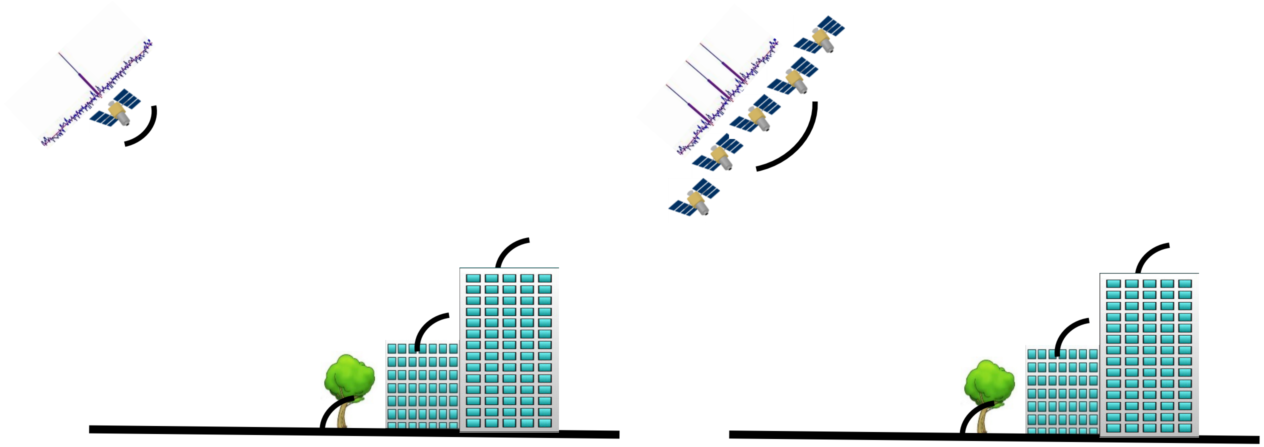

- Why multiple baselines?
  - Because: **more equations!**
  - Increased robustness against disturbances (temporal decorrelation…)
  - and/or relaxation of hypotheses required in the single baseline case
  - more unknowns are available to characterize the vertical structure of the scene

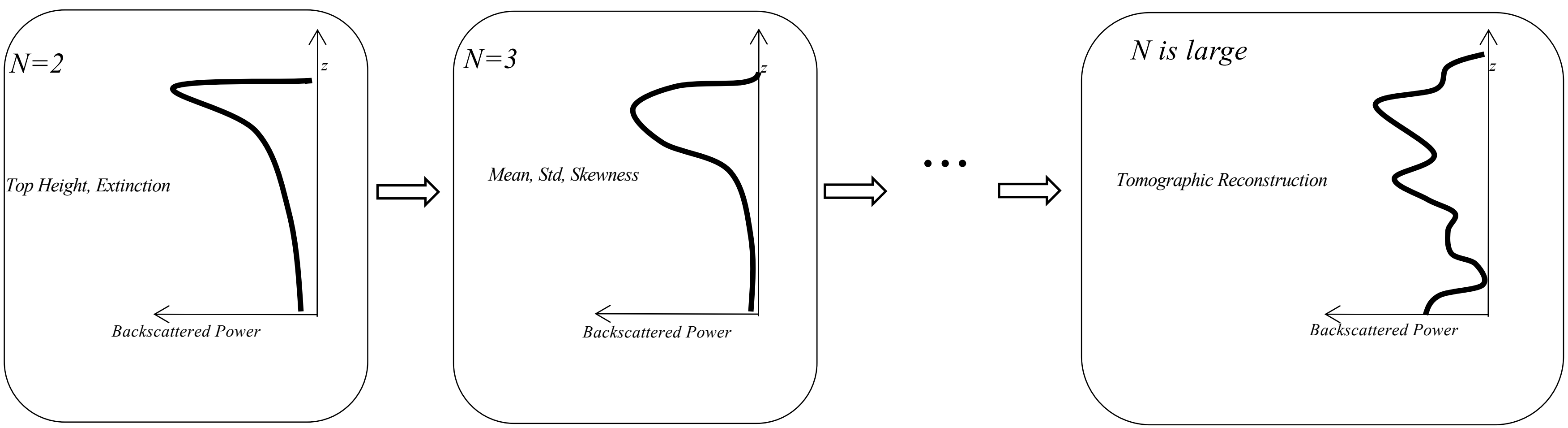

MB allow to pass from model-based inversion to full tomographic reconstruction

Tebaldini & Rocca

Rationale: Form a 2D synthetic aperture by collecting multiple SAR acquisitions acquired along parallel flight lines

- Vertical resolution ⇔ total normal baseline span
- Vertical ambiguity ⇔ normal baseline spacing

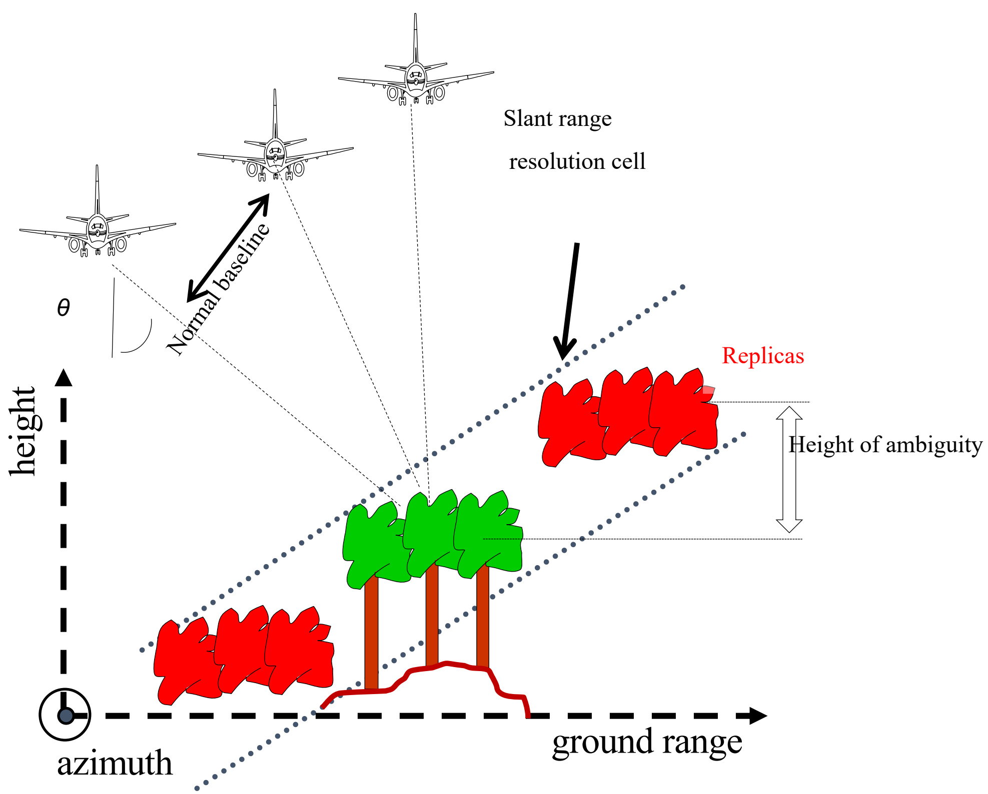

Multi-baseline (MB) systems:

- Multiple pass systems:
  - *airborne and spaceborne SARs*
- Multiple antenna systems:
  - *ground based Radars*

MB campaigns involve:

- Higher costs:
  - *spaceborne: ≈ x 1*
  - *ground based: ≈ x N*
- More sophisticated processing:
  - *see single vs multi-baseline InSAR…*

Source:
Tebaldini & Rocca

Tomographic SAR

Rationale: Form a 2D synthetic aperture by collecting multiple SAR acquisitions acquired along parallel flight lines

- Vertical resolution ⇔ total normal baseline span
- Vertical ambiguity ⇔ normal baseline spacing

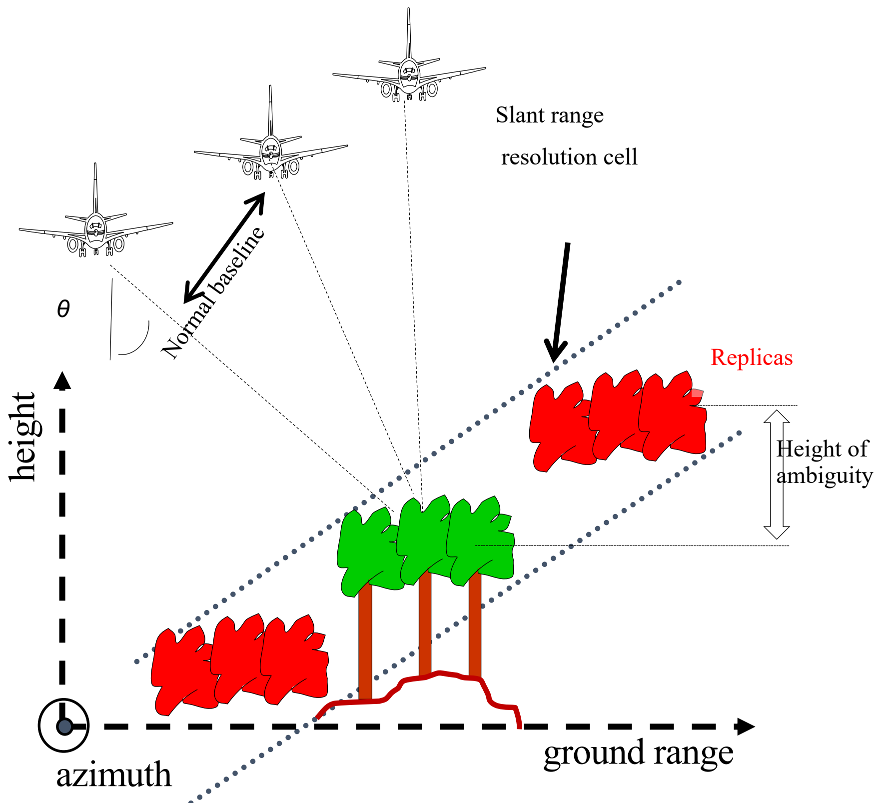

Multi-baseline (MB) systems:

- Multiple pass systems:
  - *airborne and spaceborne SARs*
- Multiple antenna systems:
  - *ground based Radars*

MB campaigns involve:

- Higher costs:
  - *spaceborne:* $\approx x\ 1$
  - *ground based:* $\approx x\ N$
- More sophisticated processing:
  - *see single vs multi-baseline InSAR…*

Source: Tebaldini & Rocca

Basic concepts

Multiple baselines ⇔ Illumination from multiple points of view

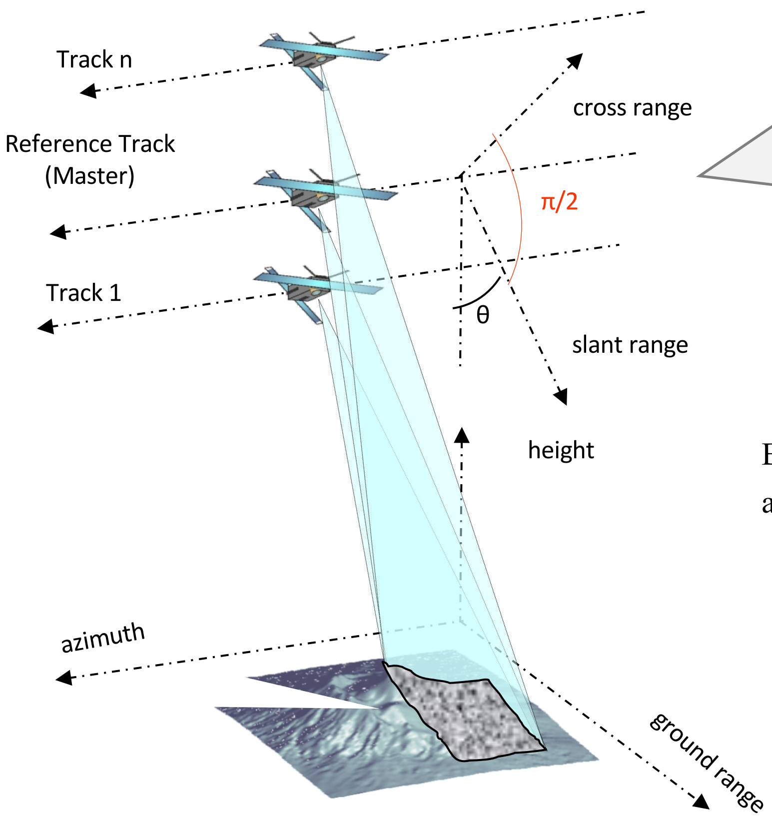

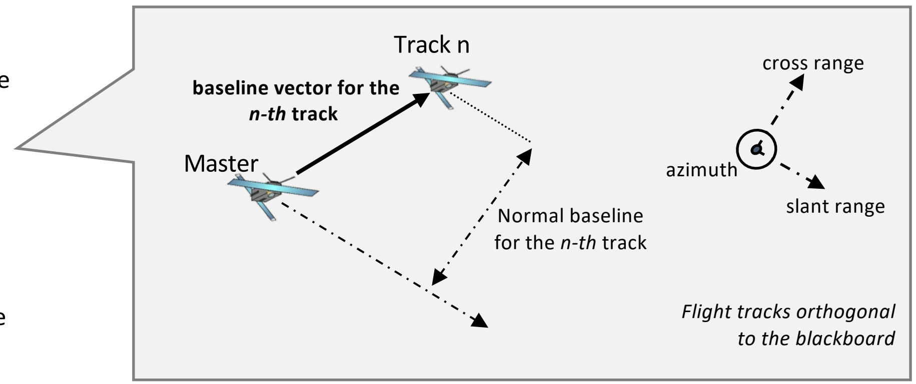

By collecting several baselines it is possible to synthesize an antenna along the cross range direction as well

⇩

3D focusing is possible in the coordinate system: *slant range, azimuth, cross range*

Source: Tebaldini & Rocca

Basic concepts

Resolution is determined by pulse bandwidth along the slant range direction, and by the lengths of the synthetic apertures in the azimuth and cross range directions

⇒The SAR resolution cell is split into **multiple layers**, according to baseline aperture

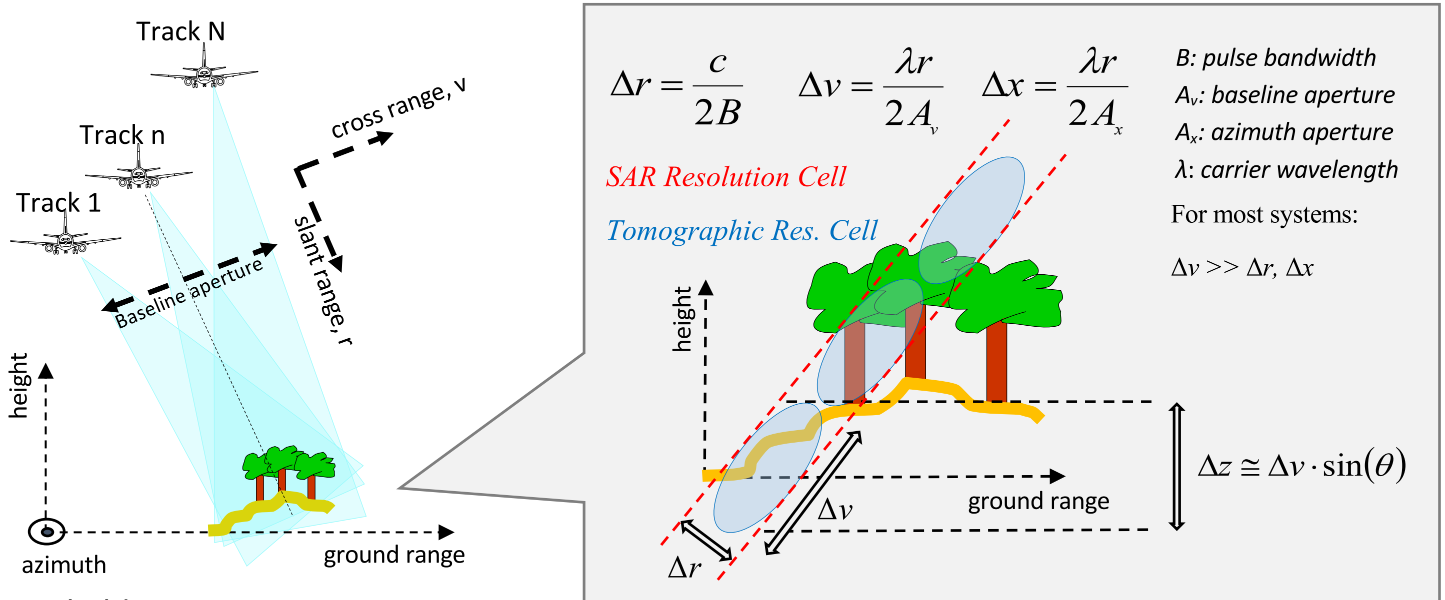

Source: Tebaldini & Rocca

TomoSAR gives access to the 3D structure

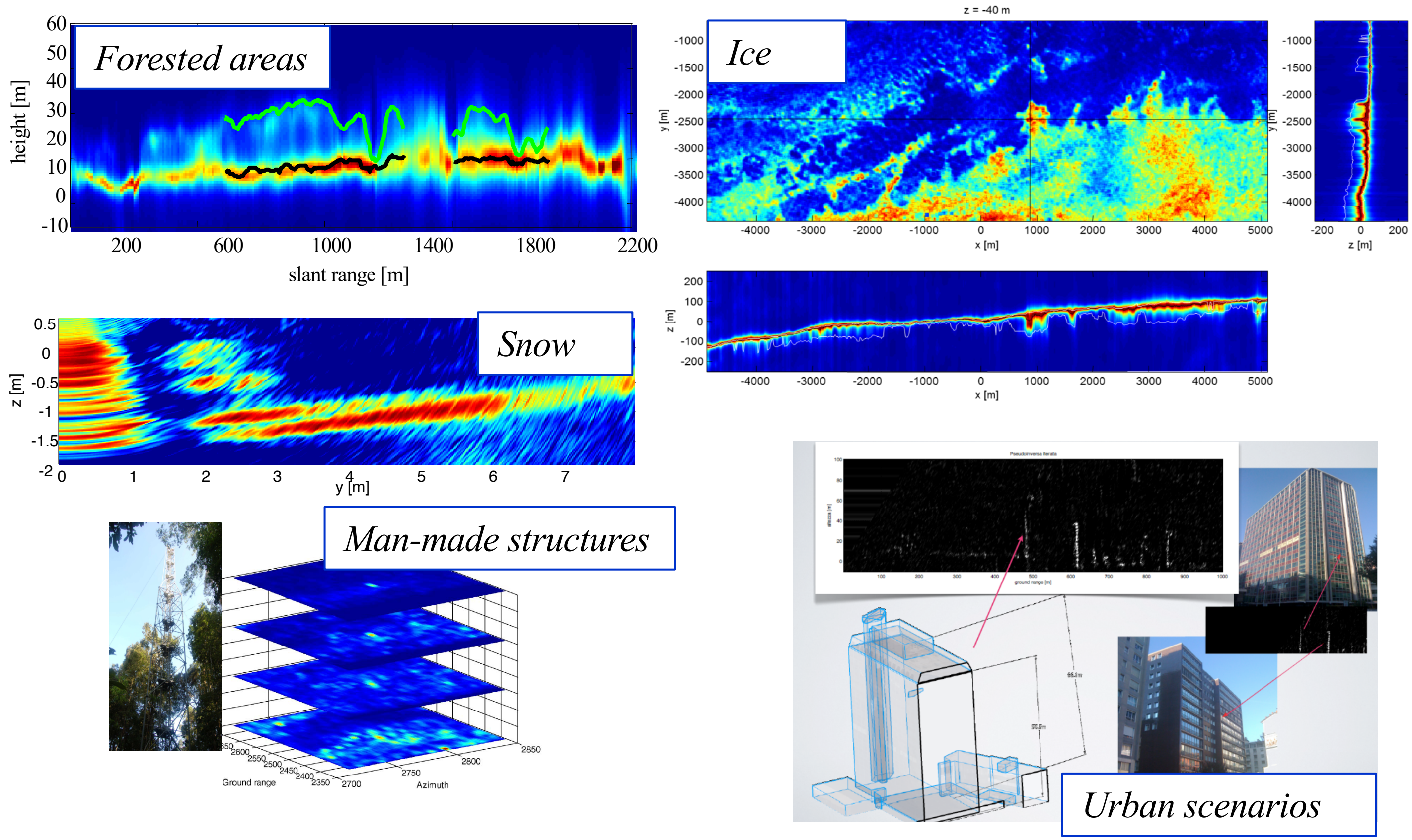

Source: Tebaldini & Rocca

Polarimetric TomoSAR over Vegetation

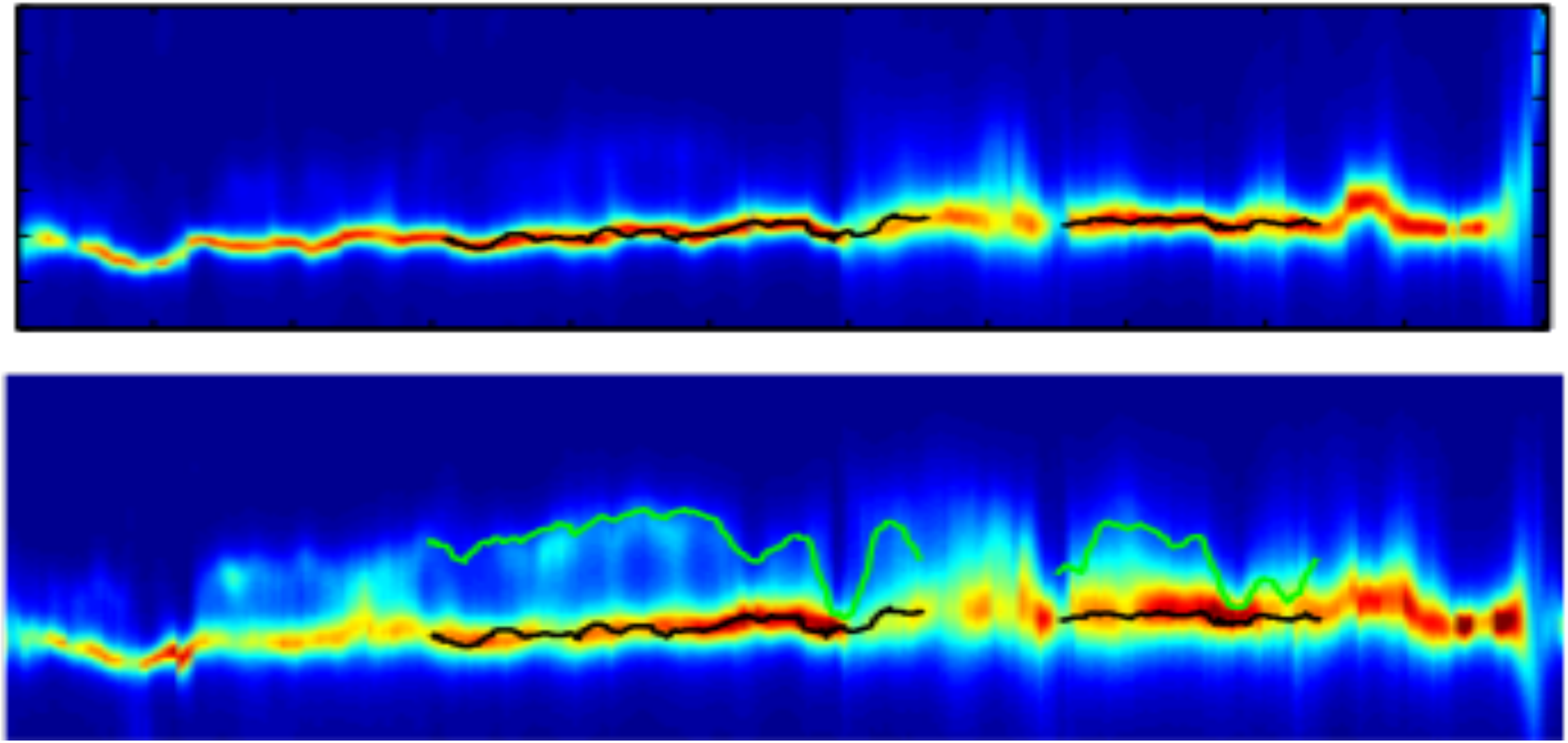

Foliage penetration

Biomass estimation

Urban TomoSAR

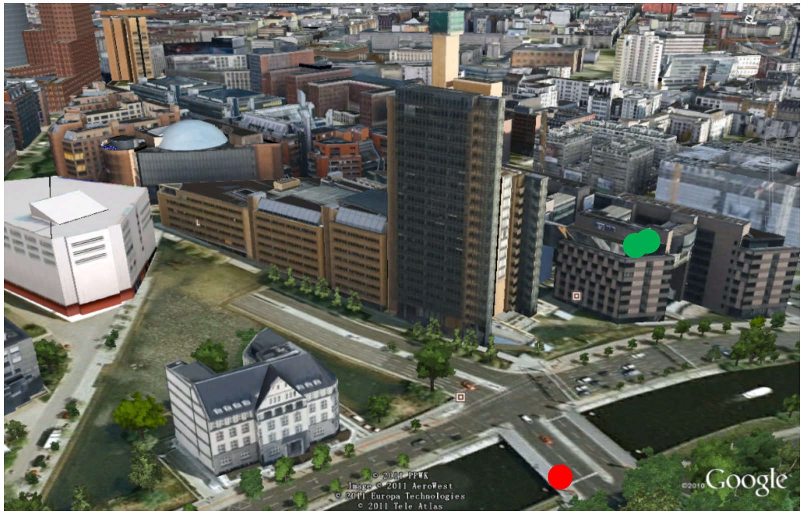

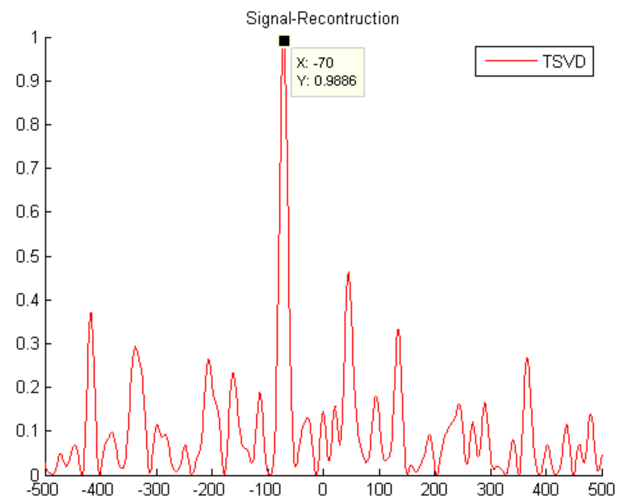

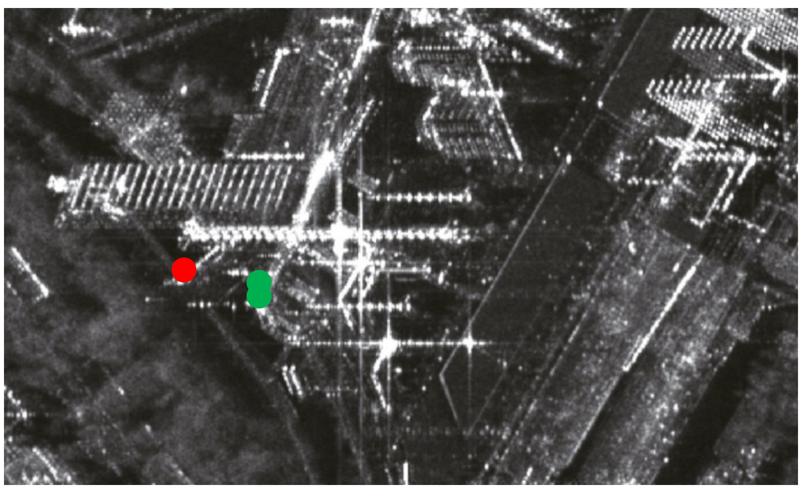

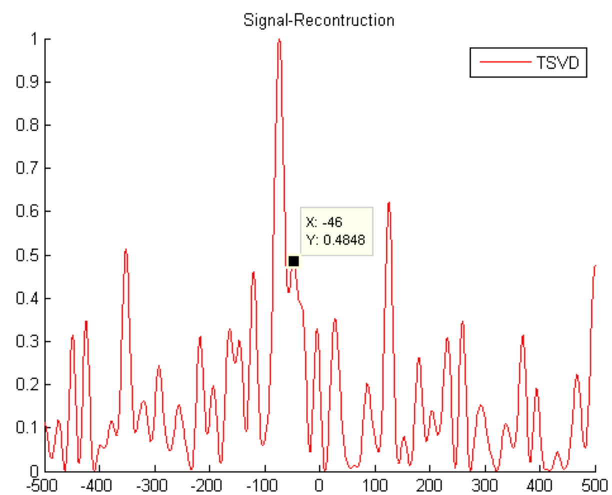

Finite number of scatterers

TomoSAR principle

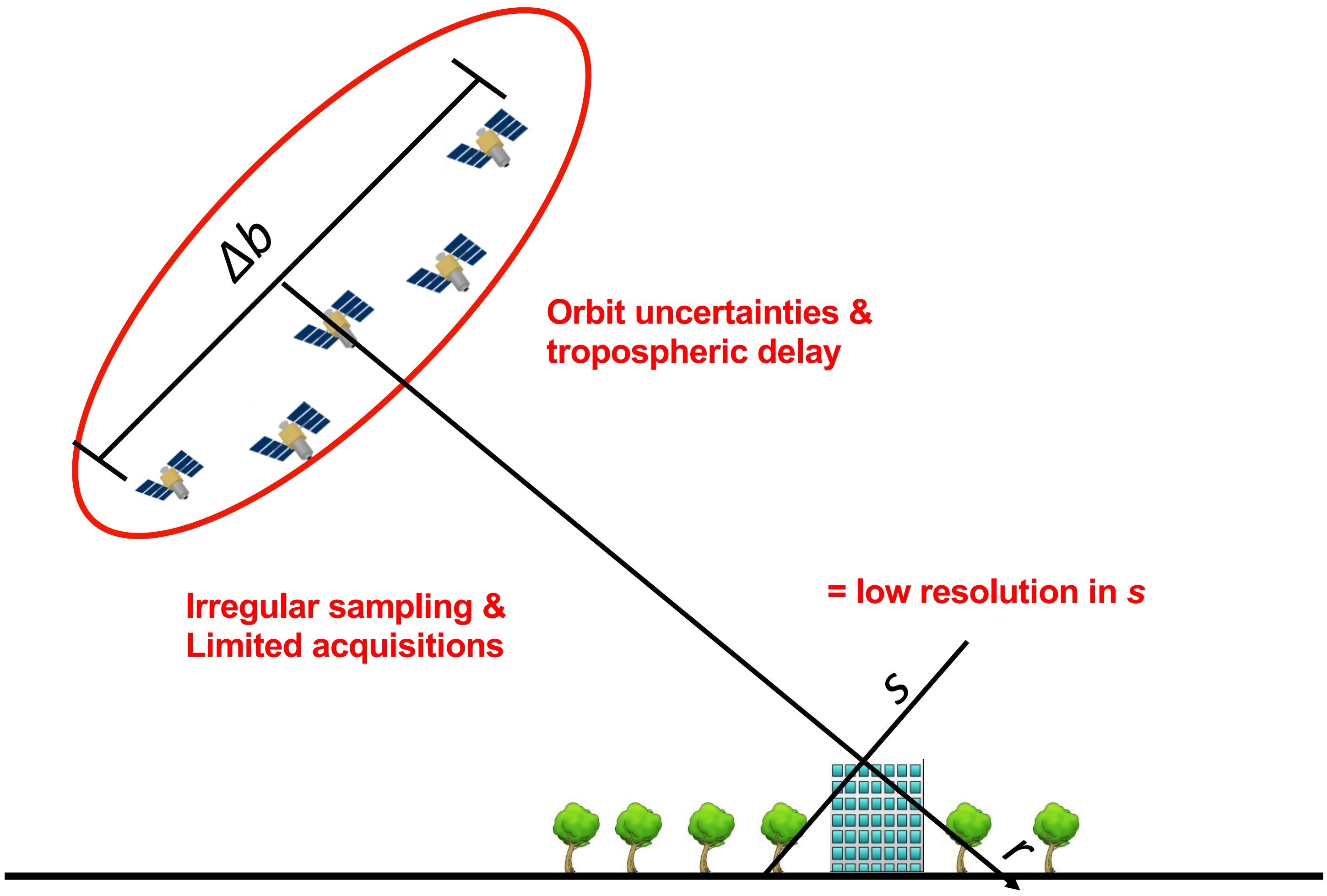

TomoSAR as spectral estimation problem

$$g_n = \int_{-a}^{a} \gamma'(s) \exp\left[-j2\pi\left(-\frac{2}{\lambda}\frac{b_{\perp n}}{\left|r_0 - b_{\parallel n}\right|}\right) s\right] ds$$

where

$$\gamma'(s) = \gamma(s)\exp[-j\frac{4\pi}{\lambda}\frac{s^2}{2\left|r_0 - b_{\parallel n}\right|}]$$

so, g_n is the Fourier transformation of $\gamma'(s)$ at position

$$f_n = -\frac{2b_{\perp n}}{\lambda\left|r_0 - b_{\parallel n}\right|} \approx -\frac{2b_{\perp n}}{\lambda r}$$

TomoSAR basics

The focused SAR image from the n^{th} pass of a specific cell is nothing else but the Fourier Transfer of the reflectivity function in the elevation direction at the position f_n.

$$g_n = \int_{-a}^{a} \gamma(s) \exp[-j2\pi f_n s]\, ds = FT[\gamma(s)]|f_n = g(f)\big|f_n$$

TomoSAR basics

The expected resolution in elevation p_s depends on the slant-range *r* and the aperture size in elevation Δb

$$p_s = \frac{\lambda r}{2\Delta b}$$

The extent of the illuminated objects and therefore the limits of the extent in elevation Δs depends on *r,* Δb, and the resolution in range p_r. In the spaceborne case, with large slant-range *r,* this is seldom a limitation (see Zhu & Bamler, 2010).

$$\Delta s \ll \frac{p_r r}{\Delta b}$$

PS-InSAR for pre-processing

- Using TomoSAR on a large area requires the removal of atmospheric effects
- This can be done using PS-InSAR
  - However, this requires a large number of PS to be found
  - Therefore, this works best in urban areas
- PS-InSAR is used for pre-processing
- Afterwards, TomoSAR can be used

PS-InSAR

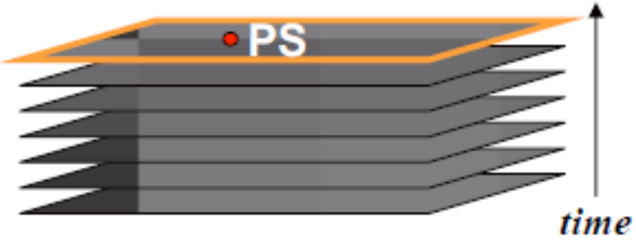

Those scatterers (called **PS**) that are coherently observed by the radar during a long period of are identified from a few tens of SAR images.

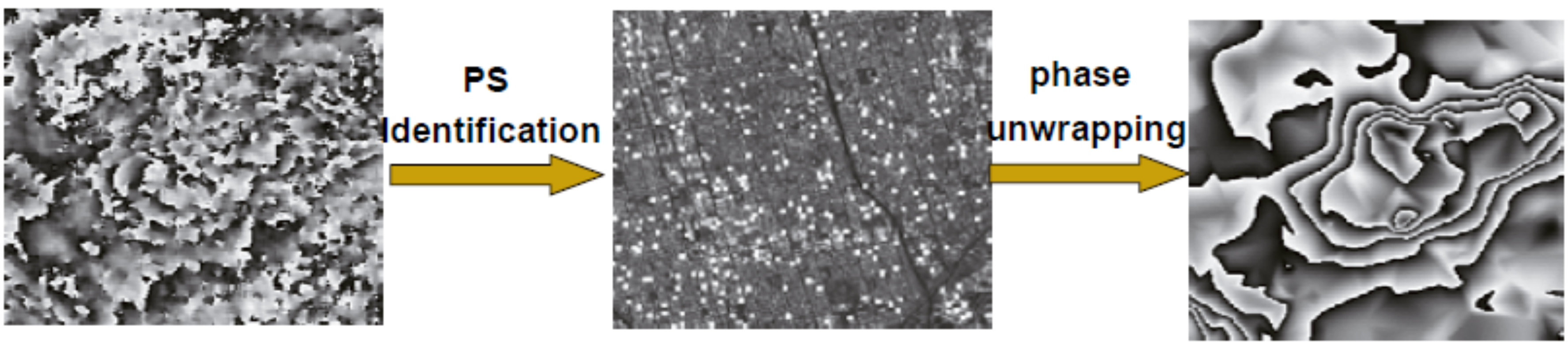

- Finding stable point-like targets --- Permanent Scatterers
- Interpolating atmosphere affection and remove it
- Estimate the elevation and deformation on PS

PS-InSAR steps

- Import
- Selection of the master image
- Co-Registration
    - Typically to a single-master
- Interferogram processing
    - Not in every implementation. Several PS-InSAR implementations only use the phases of the PS candidates
- PS candidates selection
- APS estimation
    - Typically on a subset of the PS candidates
- *PS point processing*
- *Post-processing*
- *Visualization*

Image co-registration

- Identical to the co-registration described in the InSAR section:

- Registration accuracy < 0.2 pixel is required
  - This requirement is even much higher during TOPS processing

- Different methods available
  - Based on the amplitude
  - Based on complex data – searching maximal coherence

- Slave images are resampled to the master image

- Results need to be checked and the parameters may need to be adjusted

PS candidate selection

- Classical way: amplitude dispersion index

$$d_a = \frac{StdDev_a}{Mean_a}$$

- Other possible ways, e.g. based on coherence

- Be aware: amplitude dispersion index not ideal for TomoSAR, because the existence of several scatterers in a resolution cell can increase the index

APS estimation

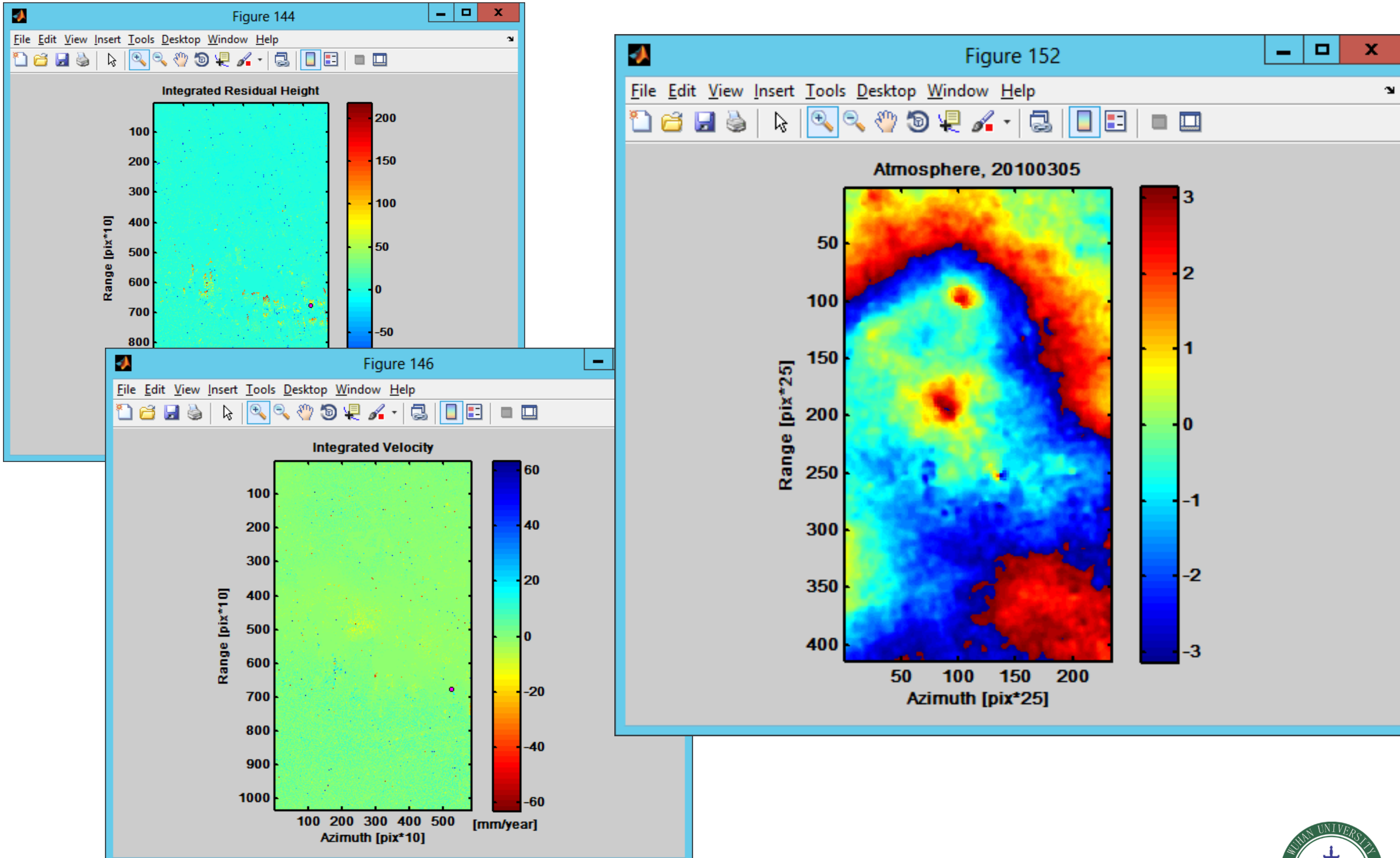

Example: SARProZ

Spectral estimators

- Beamforming:

  inverse Fourier Transform; coarse spatial resolution; radiometrically consistent

$$\hat{S}(v) = \mathbf{a}^H(v)\hat{\mathbf{R}}\mathbf{a}(v) \qquad \mathbf{a}(v) = \left[\exp\left(j\frac{4\pi}{\lambda r}b_1 v\right) \quad \exp\left(j\frac{4\pi}{\lambda r}b_2 v\right) \quad \cdots \quad \exp\left(j\frac{4\pi}{\lambda r}b_N v\right)\right]^T$$

- Capon Spectral Estimator:

  spatial resolution is greatly enhanced, at the expense of radiometric accuracy;

$$\hat{S}(v) = \frac{1}{\mathbf{a}^H(v)\hat{\mathbf{R}}^{-1}\mathbf{a}(v)}$$

- Methods based on the analysis of the Eigenstructure of **R** (MUSIC, ESPRIT…):

  determination of the dominant scatterering centers; mostly suited for urban scenarios

- **Methods based on sectorial information (Truncated SVD, PCT…):**

  optimal basis choice (e.g.: Legendre), depending on a-priori info about the scene vertical extent

- Model based methods (NLS, COMET…):

  model based; high radiometric accuracy; high computational burden; possible model mismatches

- Compressive sensing:

  localization of few scattering centers via L1 norm minimization; mostly suited for urban scenarios

Multiple scatterers

$$g_n = \sum_{k=1}^{n_p} \gamma_k e^{-j2\pi f_n s_k} + v_n \qquad n = 0, \dots, n_s$$

where

g_n = complex value observed for the n^{th} pass

γ_k= complex amplitude of k^{th} scatterer

s_k= elevation of k^{th} scatterer

$n_s + 1$= number of available images

n_p=number of scatterers inside a resolution cell

v_n=noise

f_n=frequency of sampled FT which depends on the baseline

Non-linear least-square estimation

$$\vec{g} = H(\vec{s}) \cdot \vec{x} + \vec{v}$$

$$H(\vec{s}) = \begin{bmatrix} e^{2\pi f_0 \ s_1} & \dots & e^{2\pi f_0 \ s_{n_p}} \\ \vdots & & \vdots \\ e^{2\pi f_{n_s} s_1} & \dots & e^{2\pi f_{n_s} s_{n_p}} \end{bmatrix}_{(n_s+1)\times n_p}$$

$$\vec{g} = \begin{bmatrix} g_0 \\ \vdots \\ g_n \end{bmatrix}_{(n_s+1)\times 1} \qquad \vec{x} = \begin{bmatrix} \gamma_1 \\ \vdots \\ \gamma_{n_p} \end{bmatrix}_{n_p\times 1} \qquad \vec{v} = \begin{bmatrix} v_0 \\ \vdots \\ v_n \end{bmatrix}_{(n_s+1)\times 1}$$

SVD on real data

Deutsches Zentrum
für Luft- und Raumfahrt e.V.
in der Helmholtz-Gemeinschaft

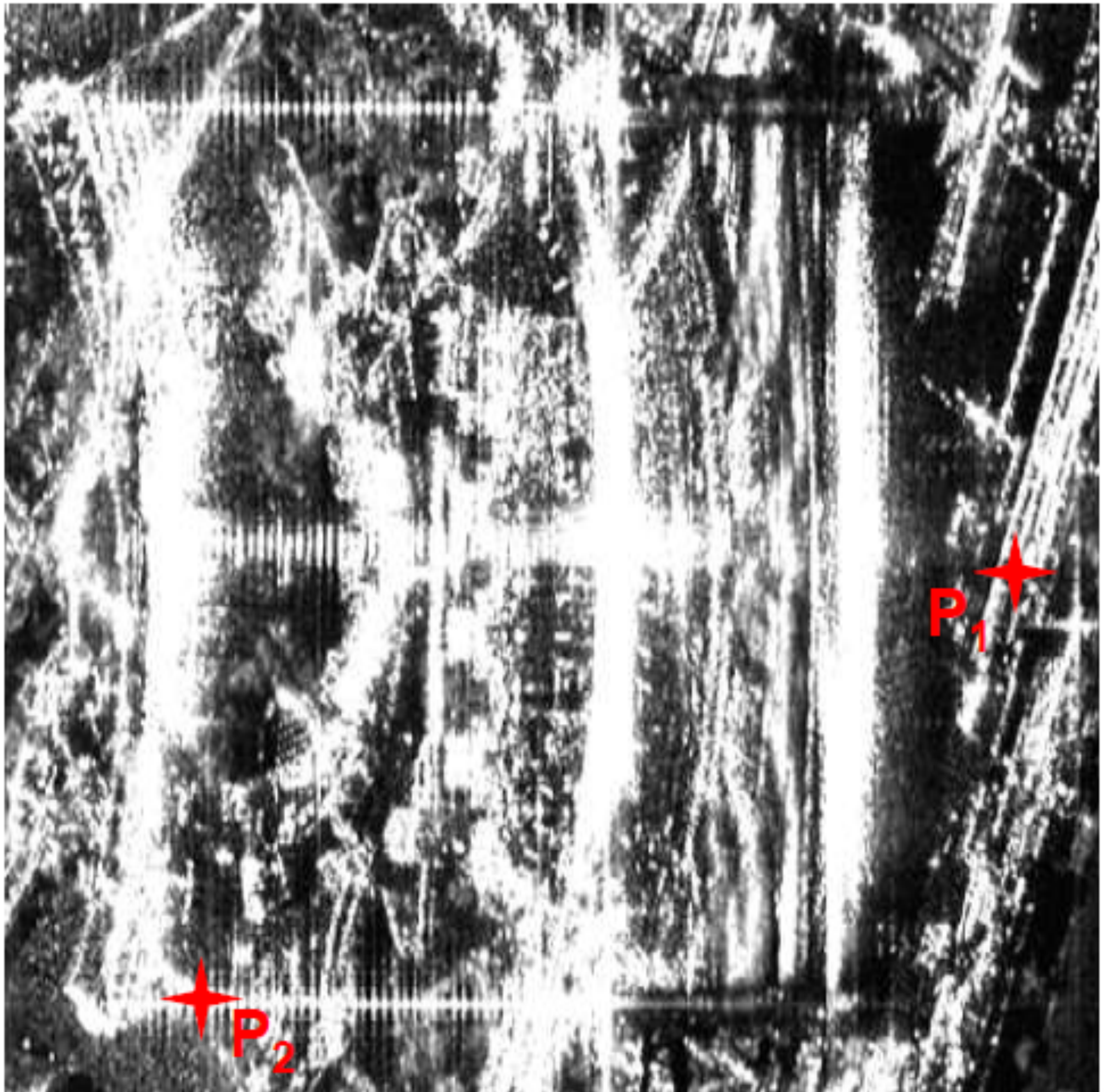

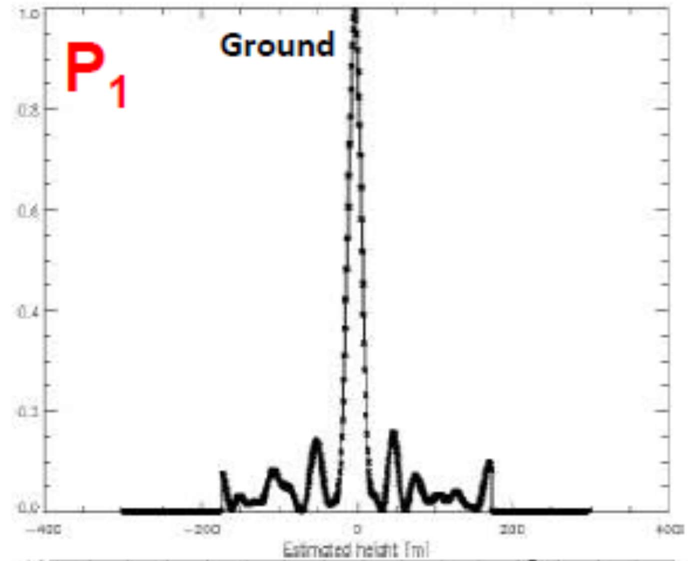

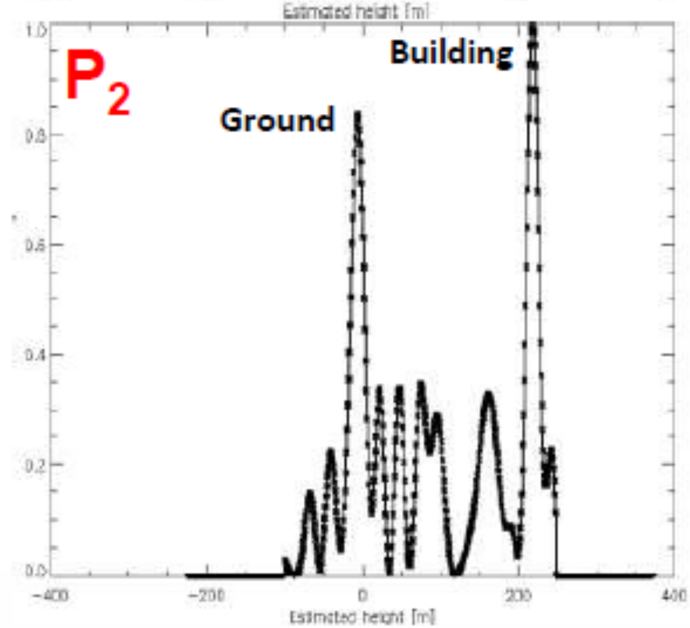

Model selection

- Selecting a statistical model for given data

too simple – order too low | appropriate model | too complex – order too high

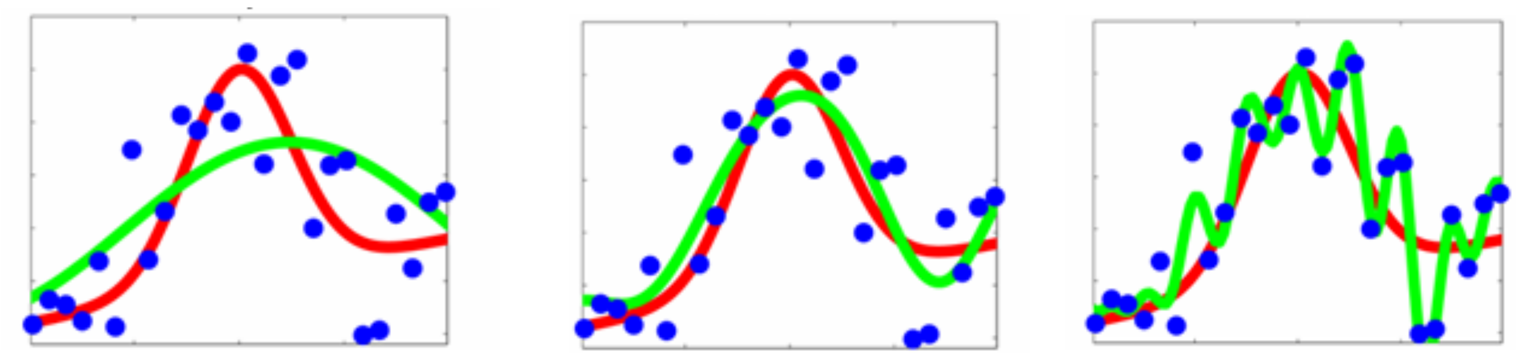

- Selecting the correct model is the model selection problem

Model selection methods

- Bayesian Information Criterion (BIC)

$$\hat{k} = \arg\max_{k} \left\{ \ln p\left(y \middle| \hat{\theta}(k), k\right) - \frac{k}{2} \ln n \right\}$$

- Akaike Information Criterion (AIC)

$$\hat{k} = \arg\min_{k} \left\{ -2\ln p\left(y \middle| \hat{\theta}(k), k\right) + 2k \right\}$$

- Minimum Description Length (MDL)

$$\hat{k} = \arg\min_{k} \left\{ -\ln p\left(y \middle| \hat{\theta}(k), k\right) + \frac{k}{2} \ln n \right\}$$

TomoSAR processing steps

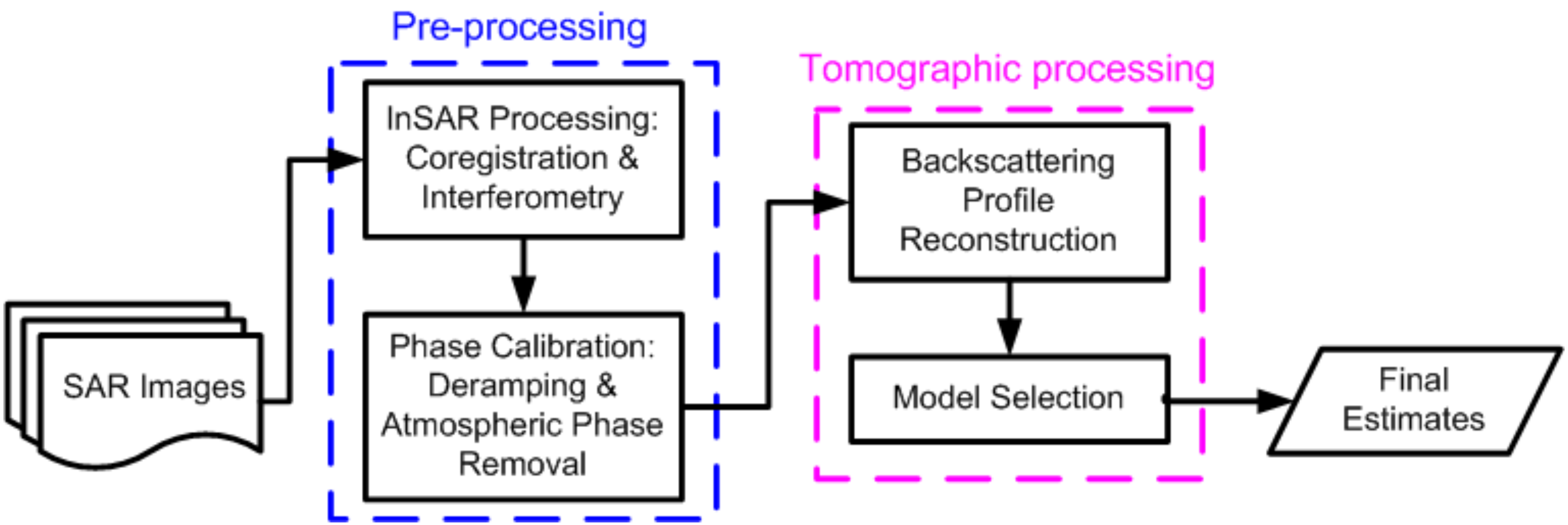

3D scatterer reconstruction

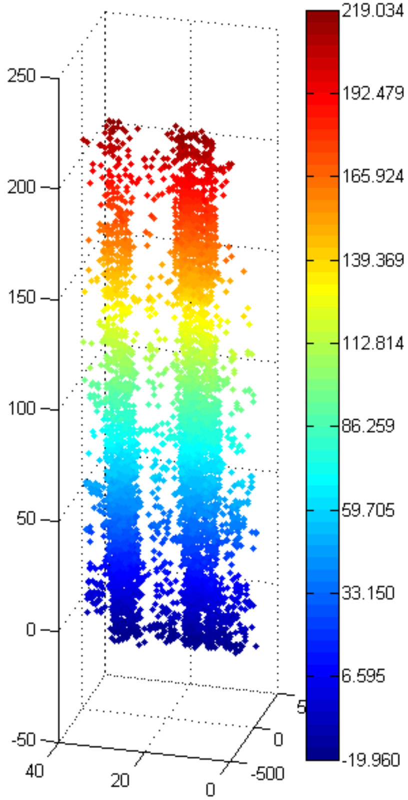

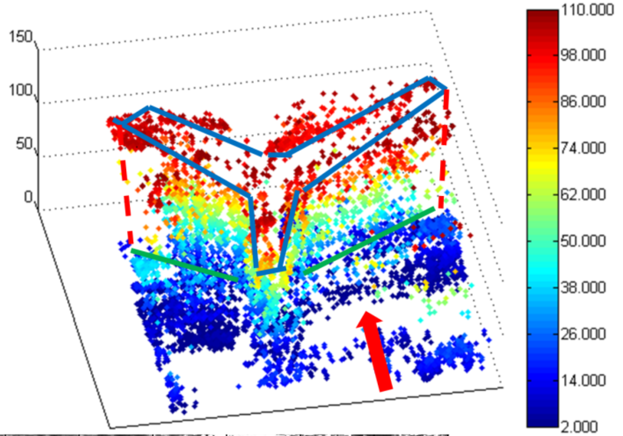

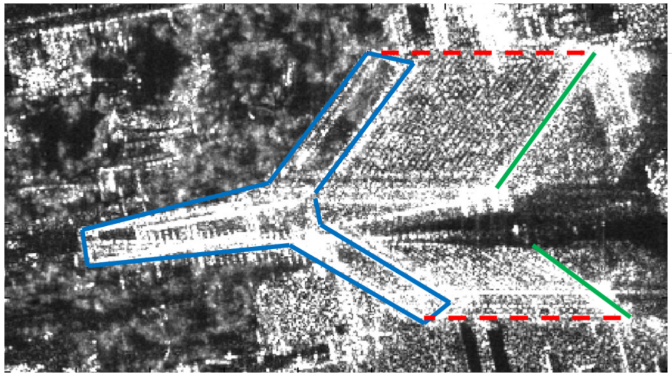

Urban TomoSAR different methods

- SVD based methods
  - SVD
  - Truncated SVD (T-SVD)
  - Wiener SVD
  - Butterworth-SVD
- Compressive Sensing based methods
  - Basis Pursuit (BP)
  - TWIST

TWIST

Another solution to SAR tomography is by L1 norm minimization, which is also the core of compressive sensing:

$$g = K \cdot \gamma + \varepsilon$$

$$\min \|\gamma\|_1 \quad \text{subject to } g = K\gamma$$

The argument listed above can be stated by

$$\Psi(\gamma) = \arg\min_{\gamma} \left\{ \frac{1}{2} \|g - K\gamma\|_2^2 + \lambda_K \|\gamma\|_1 \right\}$$

where λ_k is a weighted value adjusted according to the noise level.

TWIST

- SAR tomography with compressive sensing
  - (see Zhu, Xiaoxiang's work in the references)
- Often, TomoSAR with compressive sensing is based on Basis Pursuit (BP)
  - Very high super-resolution
  - However, time-consuming
- Alternatively: Two-Step Iterative Shrinkage Thresholding (TWIST) for TomoSAR
  - Very efficient
  - Less super-resolution capability

TWIST

When using TWIST, the least squares fitting is needed to calculate γ_0

Calculate γ_1 according to

$$\gamma_1 = \Psi(\gamma_0 + K^T(g - K\gamma_0))$$

where Ψ is the normalization equation.

If $t \geq 1$

$$\gamma_{t+1} = (1-\alpha)\gamma_{t-1} + (\alpha - \beta)\gamma_t + \beta \cdot \Psi(\gamma_t + K^T(g - K\gamma_t))$$

in which, α, β are the weighting coefficients

TomoSAR: different methods

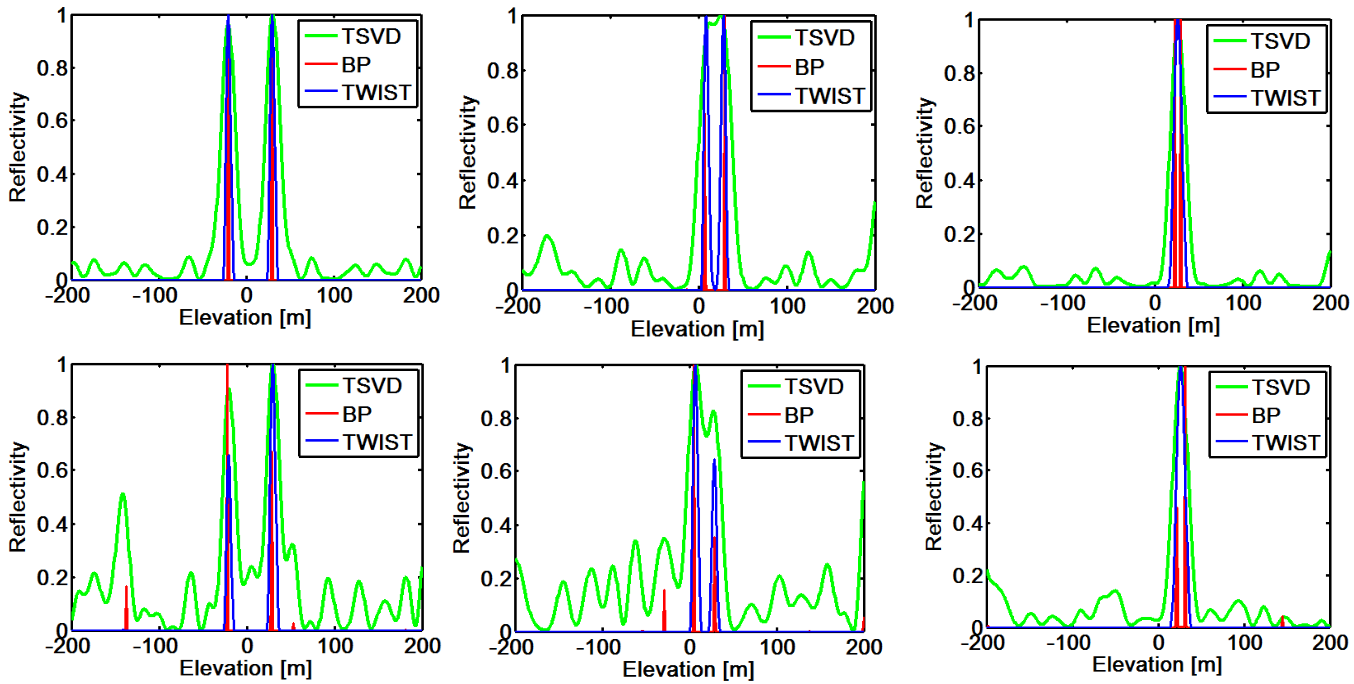

(a) s_Sc1=-20m, s_Sc2=30m;

(b) s_Sc1=8m, s_Sc2=30m;

(c) s_Sc1=23m; s_Sc2=30m

TSVD, Twist & BP

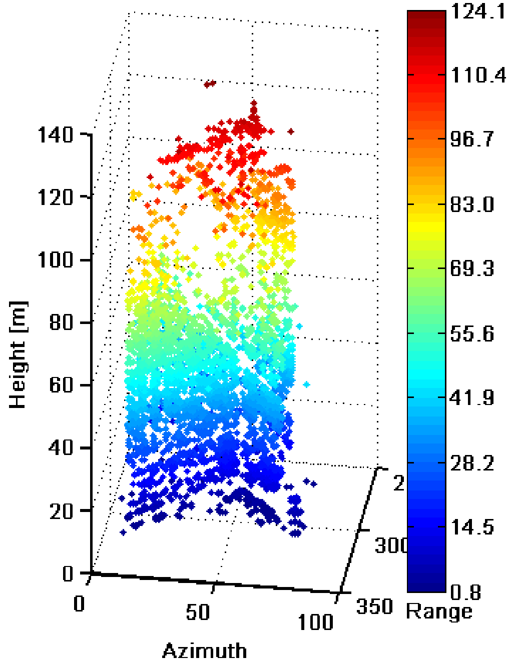

TSVD

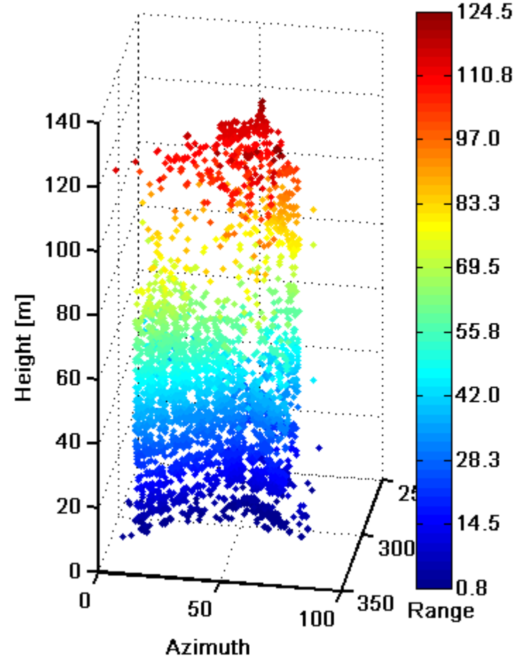

TWIST

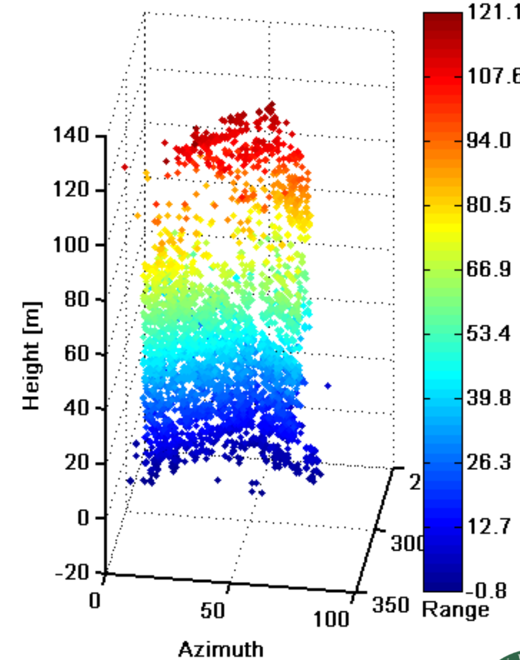

BP

TSVD, Twist & BP

（a）TSVD
85 seconds

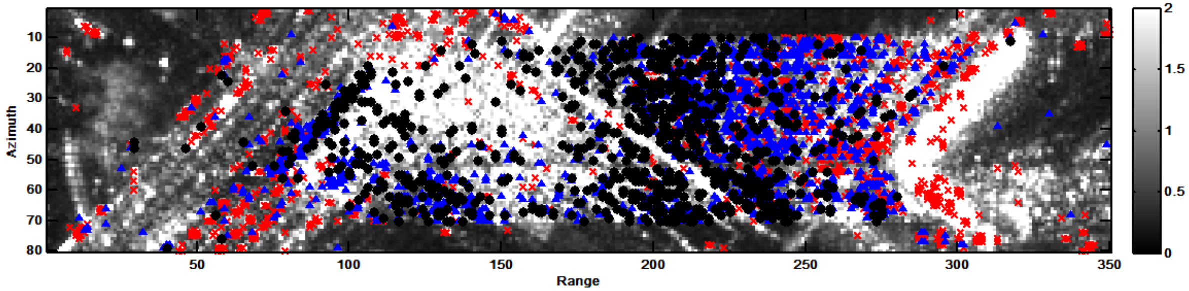

（b）TWIST
89 seconds

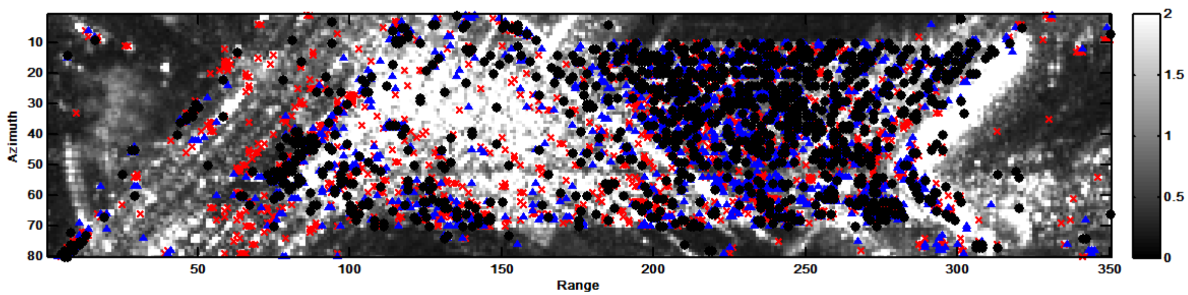

red: single;
blue: double;
black: multi

（c）BP
1378
seconds

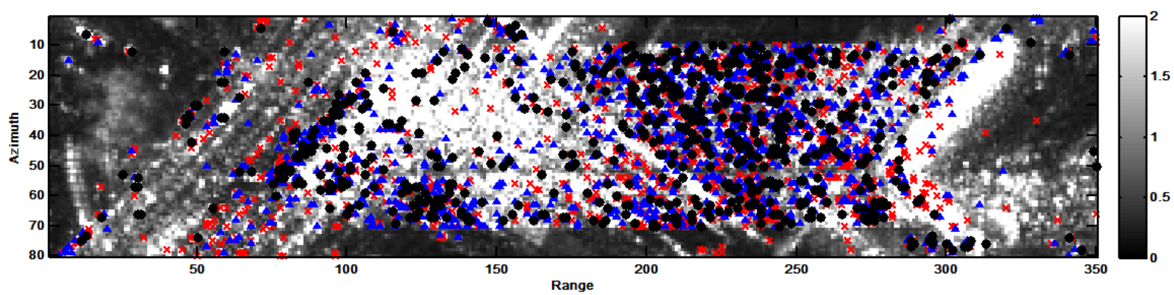

Differential TomoSAR

- Extend the model to the time-domain and include an estimation of the deformation
  - 4D TomoSAR
- Basically just an extension of the previously described method
  - Including an additional dimension for the focusing
- Can be further extended by including seasonal motion
  - Sometimes called 5D TomoSAR

D-TomoSAR

Simulation results:

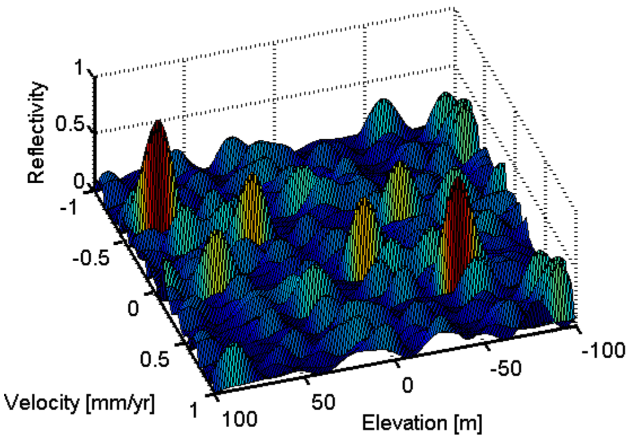

BSVD

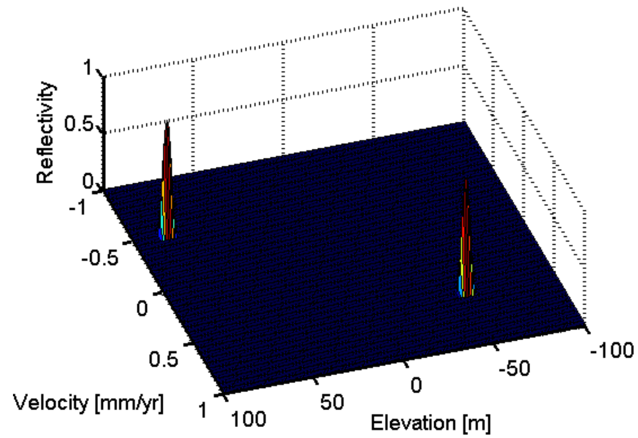

TWIST

= for D-TomoSAR, the noise suppression gets even more important

D-TomoSAR

Example: TSX stack from Las Vegas:

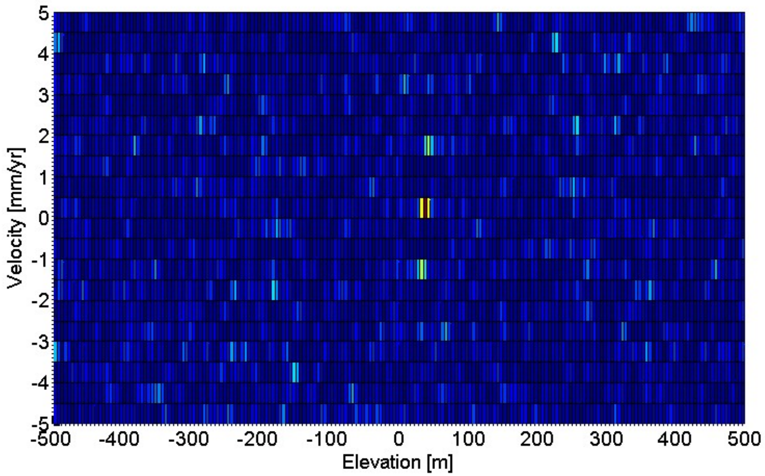

BSVD

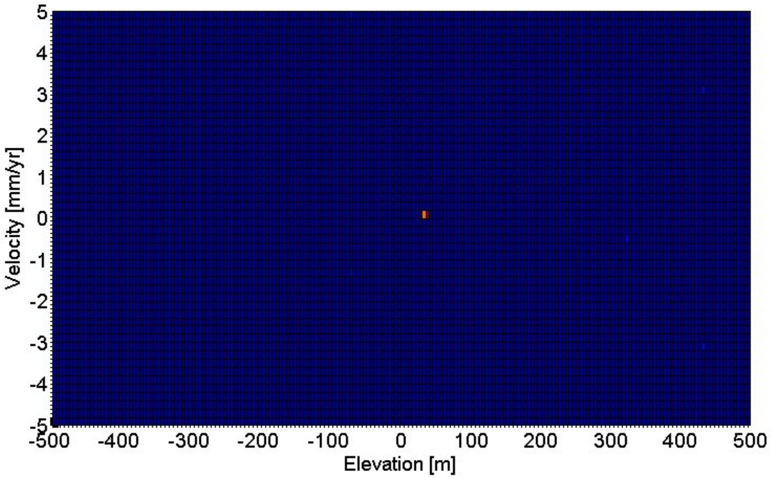

TWIST

= clear result in TWIST

Practical implementations

Due to the high computational demand for compressive sensing TomoSAR, the processing can be divided:

1. PS-InSAR for pre-processing – APS estimation
2. Basic TomoSAR processing for model estimation
3. Depending on the number of scatterers:
    - One scatterer per resolution cell: use PS-InSAR for processing
    - Two or more scatterer: use TomoSAR

Geodetic SAR tomography

- Fusion of SAR imaging geodesy and TomoSAR
- SAR imaging geodesy:
  - Very high absolute geo-positioning capability of SAR
  - Especially with TerraSAR-X due to the very precise orbit
  - see Eineder et al, Cong et al, Balss et al….
- The fusion allows getting precise *absolute* 3D positions

Geodetic SAR tomography

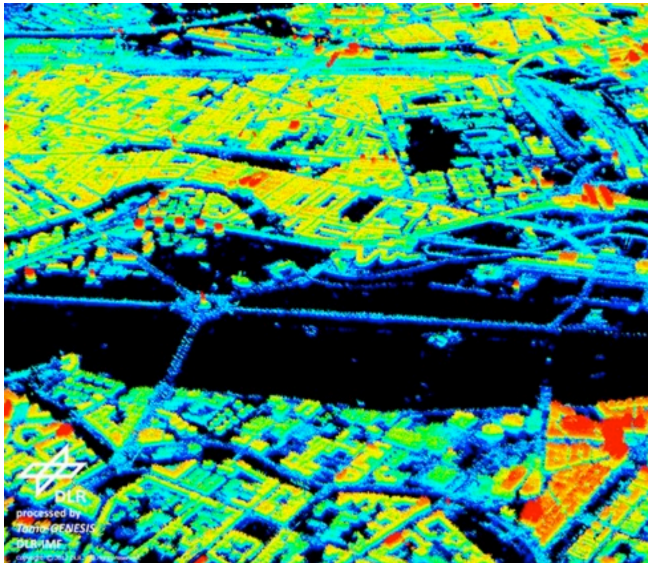

from Zhu et al, 2016 – 3D absolute positioned TomoSAR point cloud from Berlin

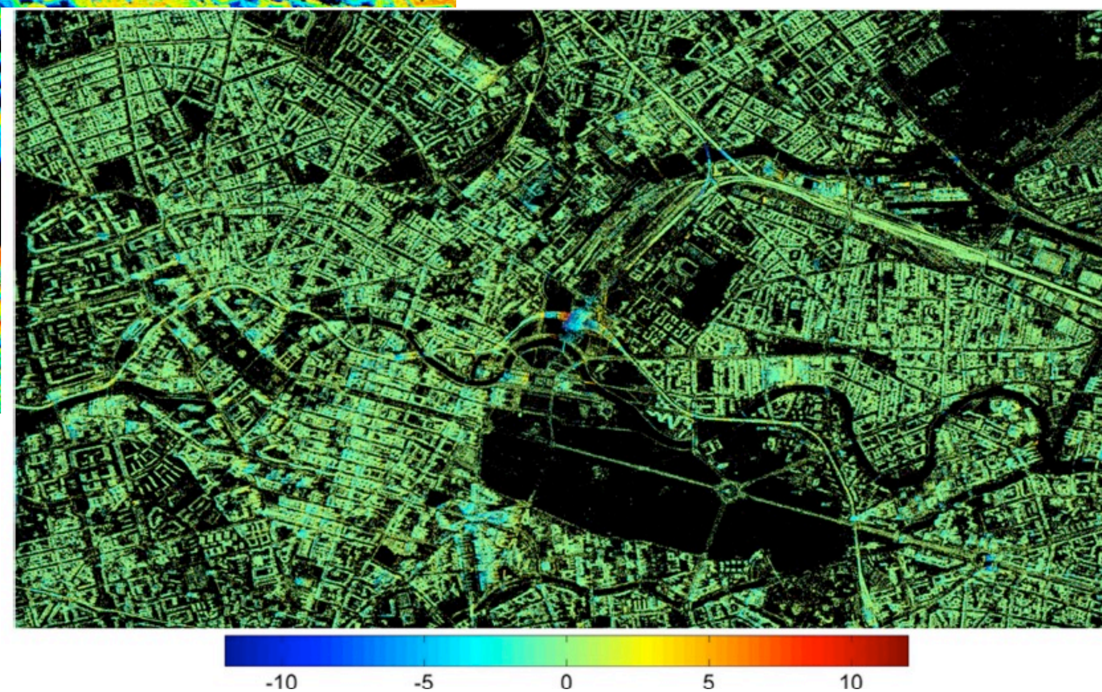

from Zhu et al, 2016 – Amplitude of the seasonal motion derived from one stack

References

❖Reigber, A.; Moreira, A.; , "First demonstration of airborne SAR tomography using multibaseline L-band data," Geoscience and Remote Sensing, IEEE Transactions on , vol.38, no.5, pp.2142-2152, Sep 2000

❖G. Fornaro, F. Serafino, and F. Soldovieri, “Three-dimensional focusing with multipass SAR data,” *IEEE Trans. Geosci. Remote Sens.*, vol. 41, no. 3, pp. 507–517, Mar. 2003.

❖F. Lombardini, “Differential tomography: a new framework for SAR interferometry,” *IEEE Trans. Geosci. Remote Sens.*, vol. 43, no. 1, pp. 37–44, Jan. 2005.

❖G. Fornaro and F. Serafino, “Imaging of Single and Double Scatterers in Urban Areas via SAR Tomography,” *IEEE Trans. Geosci. Remote Sens.*, vol. 44, no. 12, pp. 3497–3505, Dec. 2006.

❖F. Lombardini and M. Pardini, “3-D SAR Tomography: The Multibaseline Sector Interpolation Approach,” *IEEE Geosci. Remote Sens. Lett.*, vol. 5, no. 4, pp. 630–634, Oct. 2008.

❖G. Fornaro, D. Reale, and F. Serafino, “Four-Dimensional SAR Imaging for Height Estimation and Monitoring of Single and Double Scatterers,” *IEEE Trans. Geosci. Remote Sens.*, vol. 47, no. 1, pp. 224–237, Jan. 2009.

❖ X. X. Zhu and R. Bamler, “Tomographic SAR Inversion by L1-Norm Regularization—The Compressive Sensing Approach,” *IEEE Trans. Geosci. Remote Sens.*, vol. 48, no. 10, pp. 3839–3846, Oct. 2010.

❖X. X. Zhu and R. Bamler, “Let’s Do the Time Warp: Multicomponent Nonlinear Motion Estimation in Differential SAR Tomography,” *IEEE Geosci. Remote Sens. Lett.*, vol. 8, no. 4, pp. 735–739, 2011.

❖X. X. Zhu and R. Bamler, “Very High Resolution Spaceborne SAR Tomography in Urban Environment,” *IEEE Trans. Geosci. Remote Sens.*, vol. 48, no. 12, pp. 4296–4308, 2010.

❖X. X. Zhu and R. Bamler, “Super-Resolution Power and Robustness of Compressive Sensing for Spectral Estimation With Application to Spaceborne Tomographic SAR,” *IEEE Trans. Geosci. Remote Sens.*, vol. 50, no. 1, pp. 247–258, 2011.

❖ X. X. Zhu and R. Bamler, “Demonstration of Super-Resolution for Tomographic SAR Imaging in Urban Environment,” *IEEE Trans. Geosci. Remote Sens.*, vol. 50, no. 8, pp. 3150–3157, Aug. 2012.

❖F. Lombardini and M. Pardini, “Superresolution Differential Tomography: Experiments on Identification of Multiple Scatterers in Spaceborne SAR Data,” *IEEE Trans. Geosci. Remote Sens.*, vol. 50, no. 4, pp. 1117–1129, 2012.

❖D. Reale, G. Fornaro, and A. Pauciullo, “Extension of 4-D SAR Imaging to the Monitoring of Thermally Dilating Scatterers,” *IEEE Trans. Geosci. Remote Sens.*, vol. 51, no. 12, pp. 5296–5306, 2013.

❖G. Fornaro, A. Pauciullo, D. Reale, and S. Verde, “Multilook SAR Tomography for 3-D Reconstruction and Monitoring of Single Structures Applied to COSMO-SKYMED Data,” *IEEE J. Sel. Top. Appl. Earth Obs. Remote Sens.*, vol. 7, no. 7, pp. 2776–2785, Jul. 2014.

❖X. X. Zhu, S. Montazeri, C. Gisinger, R. F. Hanssen, and R. Bamler, “Geodetic SAR Tomography,” *IEEE Trans. Geosci. Remote Sens.*, vol. 54, no. 1, pp. 18–35, Jan. 2016.

Tomographic scene reconstruction

Assuming typical airborne or spaceborne MB geometries, SAR Tomography can be formulated according to one simple principle:

Each focused SLC SAR image is obtained as the Fourier Transform of the scene complex reflectivity along the cross-range coordinate

$$y_n(r,x) = \int s(r,x,v)\exp\left(-j\frac{4\pi}{\lambda r}b_n v\right)dv$$

$y_n(r,x)$: SLC pixel in the *n-th* image

$s(r,x,v)$: average complex reflectivity of the scene within the SAR 2D resolution cell at (r,x)

b_n : normal baseline for the *n-th* image

λ : carrier wavelength

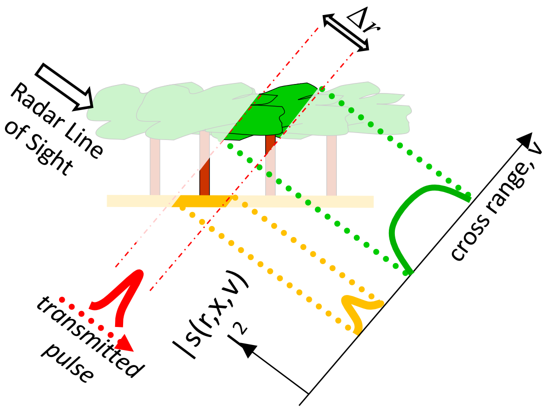

$\Rightarrow$ The cross-range distribution of the complex reflectivity can be retrieved through Fourier-based techniques

Source: Tebaldini & Rocca

Tomographic scene reconstruction

Example: Tomographic reconstruction of a forest scenario

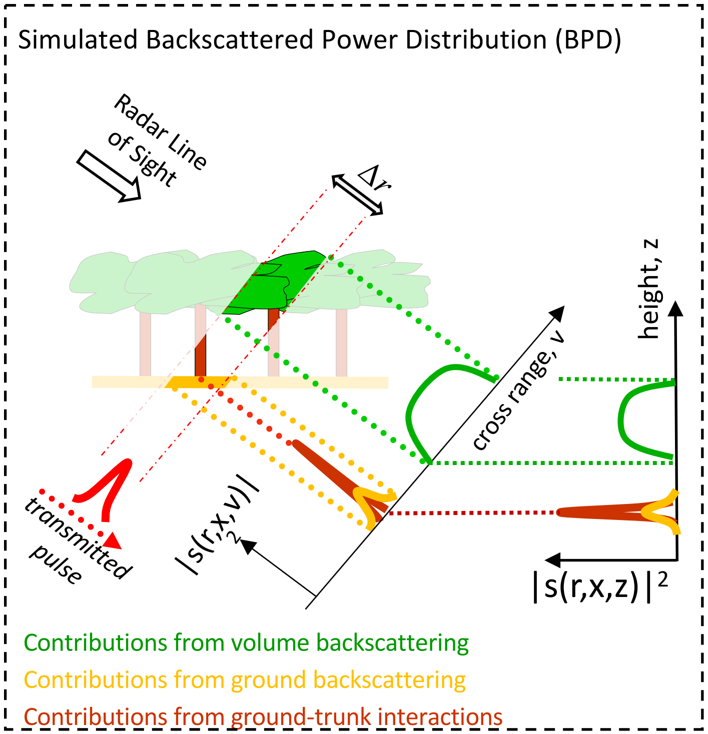

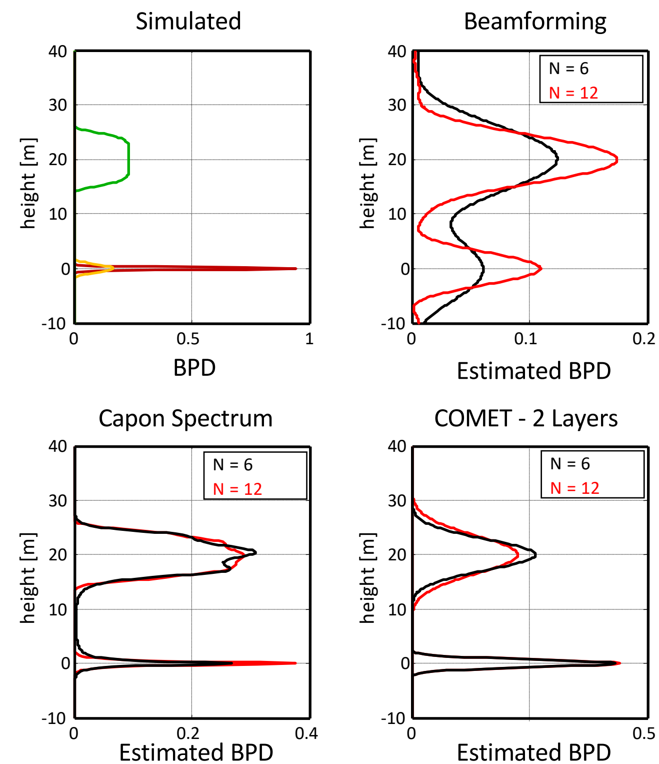

Source: Tebaldini & Rocca

BIOMASS tomographic phase

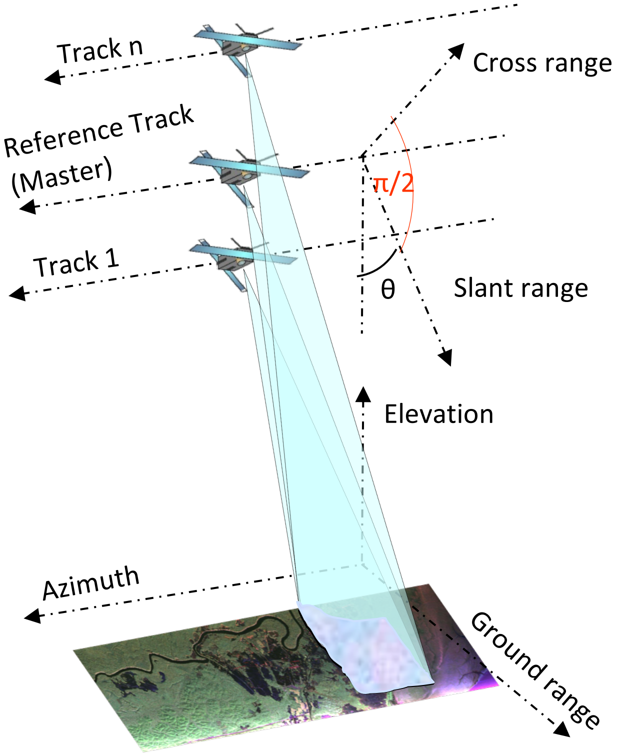

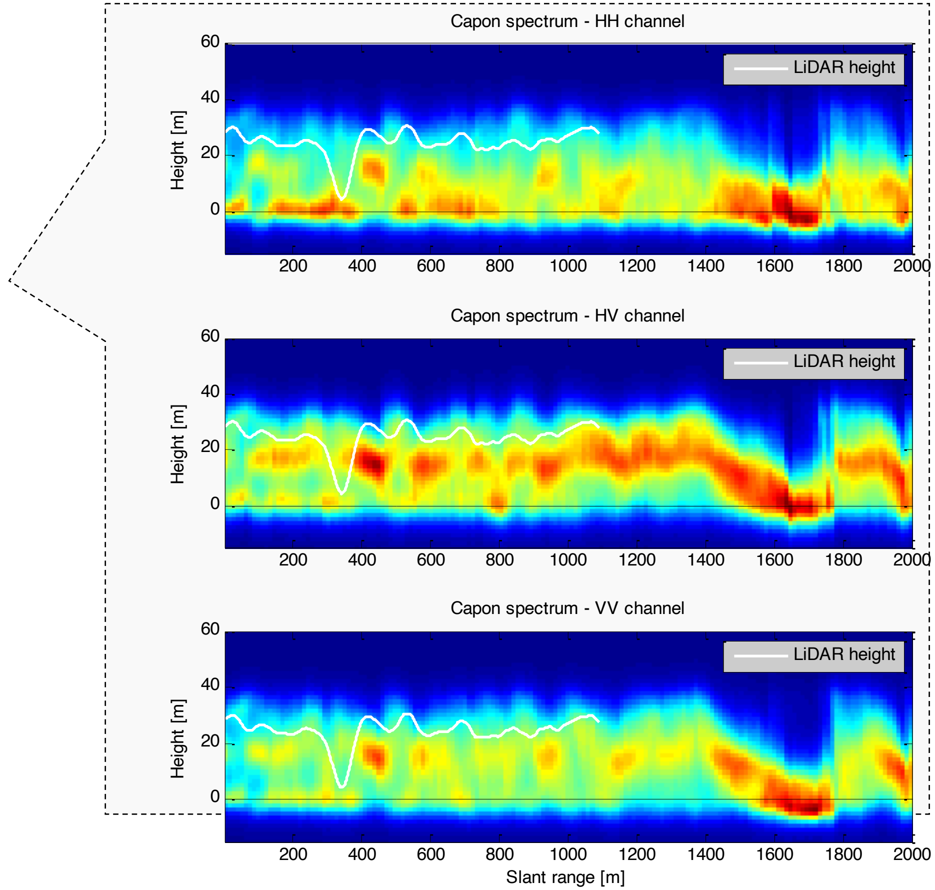

Source:
Tebaldini & Rocca

Tomographic analysis: TropiSAR

A closer look…

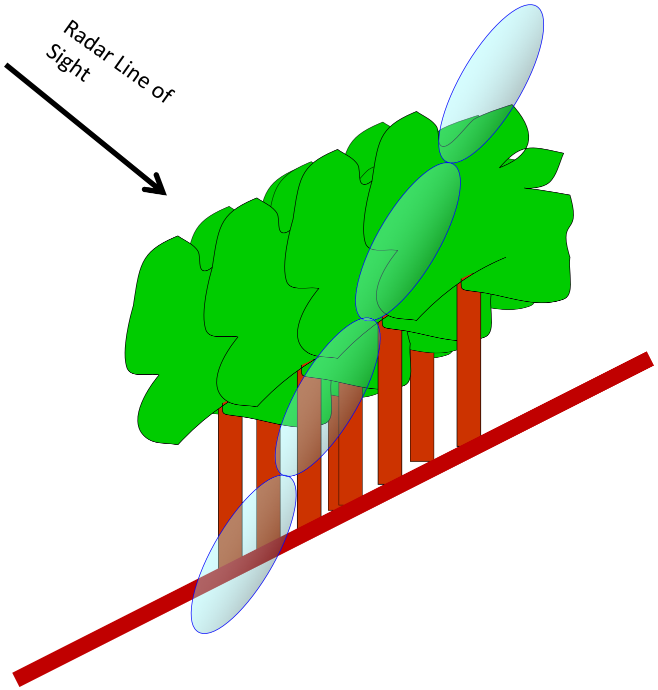

Source: Rocca

Tomographic analysis: TropiSAR

A closer look…

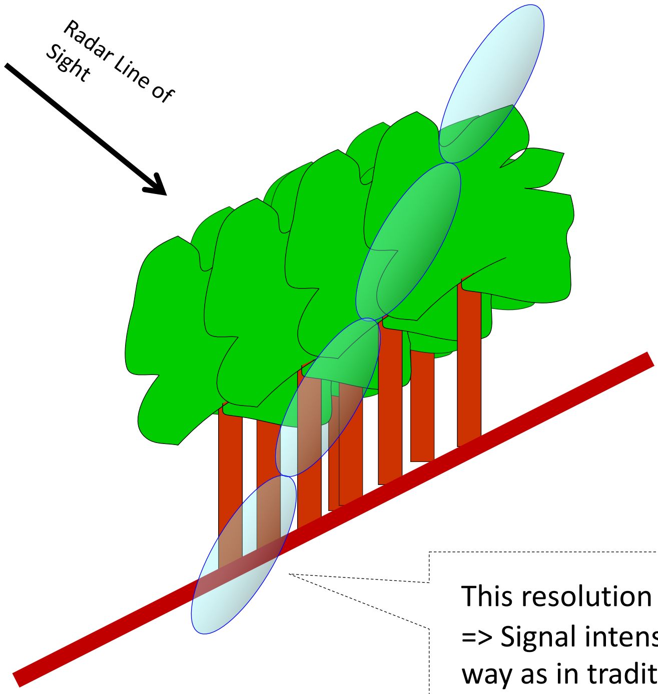

This resolution cell gathers contributions from terrain only.
=> Signal intensity in this cell is affected by terrain slope the same way as in traditional SAR images of bare surfaces

Source: Rocca

Tomographic analysis: TropiSAR

A closer look…

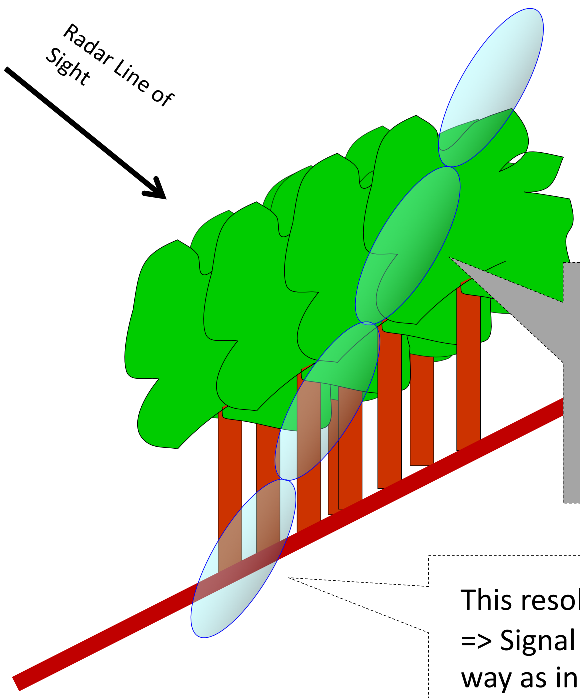

This cell is completely within the volume layer, independently on volume orientation w.r.t. the Radar LOS.
=> Signal intensity in this cell is independent of terrain slope

This resolution cell gathers contributions from terrain only.
=> Signal intensity in this cell is affected by terrain slope the same way as in traditional SAR images of bare surfaces

Source: Rocca

Tomographic analysis: TropiSAR

A closer look…

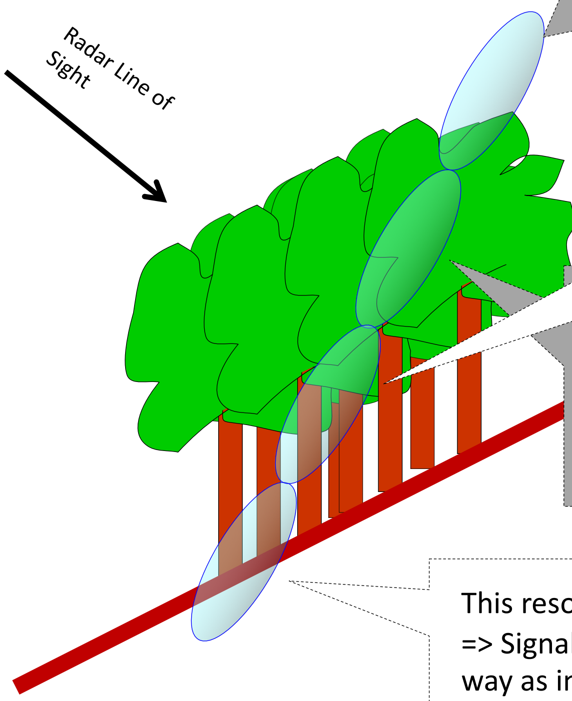

The scattering volume within cells at the boundaries of the vegetation layer depends on volume orientation w.r.t. the Radar LOS.
=> Signal intensity in this cell is affected by terrain slope in a similar way as the cell corresponding to the ground layer.

This cell is completely within the volume layer, independently on volume orientation w.r.t. the Radar LOS.
=> Signal intensity in this cell is independent of terrain slope

This resolution cell gathers contributions from terrain only.
=> Signal intensity in this cell is affected by terrain slope the same way as in traditional SAR images of bare surfaces

Source: Rocca

Tomographic analysis: TropiSAR

Co-polar signature at the ground layer reveals ground-trunk double bounce interactions dominate the signal from flat areas *despite* the presence of a 40 m dense tropical forest

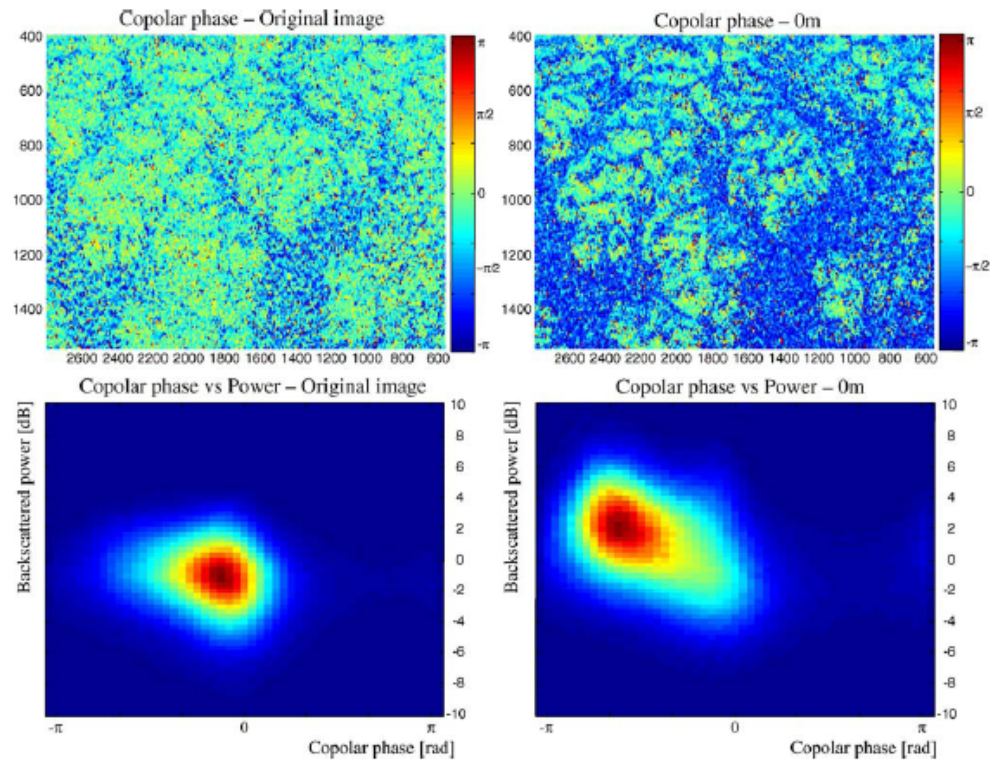

Source: Rocca

Towards BIOMASS

- **The scattering mechanisms at P-band in a very dense tropical forest:**

  Ground scattering is strongly visible and double bounces in flat terrain topography are visible everywhere.

  Volume scattering is significantly related to the high range biomass

- **It was found that scattering contributions from about 30 m above ground exhibit high sensitivity to forest biomass value ranging *from 250 t/ha to 450 t/ha*.**

- **SAR tomography** allows to map not only **vertical forest structure** but also **biomass.**

Forest temporal decorrelation

P-band SAR tomography

- **key tool to *SEE* through the forest**
- **suitable long wavelength to penetrate the dense forest layer**
- **key indicator to tropical forest biomass**

Orbit constraint: temporal decorrelation

- **Revisit time ≥ 1 day in a sun synchronous satellite configuration**
- **Forest scattering changes with time**

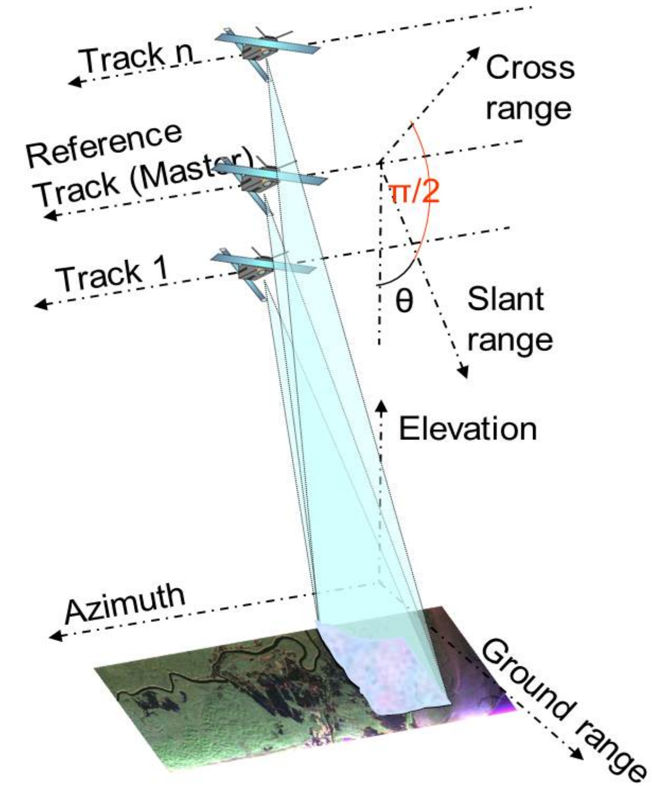

GOAL: Study the temporal decorrelation of scattering mechanisms of the radar signal in a tropical forest as a function of height and polarization.

References

Polarimetric and tomographic phenomenology of forests

❖ Reigber, A.; Moreira, A.; , "First demonstration of airborne SAR tomography using multibaseline L-band data," *Geoscience and Remote Sensing, IEEE Transactions on* , vol.38, no.5, pp.2142-2152, Sep 2000

❖ Mariotti d'Alessandro, M.; Tebaldini, S.; , "Phenomenology of P-Band Scattering From a Tropical Forest Through Three-Dimensional SAR Tomography," *Geoscience and Remote Sensing Letters, IEEE* , vol.9, no.3, pp.442-446, May 2012

❖ Frey, O.; Meier, E.; , "3-D Time-Domain SAR Imaging of a Forest Using Airborne Multibaseline Data at L- and P-Bands," *Geoscience and Remote Sensing, IEEE Transactions on* , vol.49, no.10, pp.3660-3664, Oct. 2011

Multi-layer optimization

❖ S. Sauer, L. Ferro-Famil, A. Reigber, E. Pottier, "Multi-aspect POL-InSAR 3D Urban Scene Reconstruction at L-Band", *Eusar 2008*

❖ Y. Huang, L. Ferro-Famil, A. Reigber, "Under Foliage Object Imaging Using SAR Tomography and Polarimetric Spectral Estimators", *Eusar 2010*

Coherence optimization

❖ M. Neumann, L. Ferro-Famil, A. Reigber, "Multibaseline Polarimetric SAR Interferometry Coherence Optimization", *IEEE Geoscience and Remote Sensing Letters*, 2008

❖ E. Colin, C. Titin-Schnaider, W. Tabbara, "An Interferometric Coherence Optimization Method in Radar Polarimetry for High-Resolution Imagery", *IEEE Transactions on Geoscience and Remote Sensing*, 2006

SKP decomposition: theory, algorithms and physical implications

❖ S. Tebaldini, "Algebraic Synthesis of Forest Scenarios from Multi-Baseline PolInSAR Data", *IEEE Transactions on Geoscience and Remote Sensing*, 2009

❖ Tebaldini, S.; Rocca, F.; , "Multibaseline Polarimetric SAR Tomography of a Boreal Forest at P- and L-Bands," *Geoscience and Remote Sensing, IEEE Transactions on* , vol.50, no.1, pp.232-246, Jan. 2012

Questions?

balz@whu.edu.cn